CEReS
Center for Environmental Remote Sensing
Chiba University, Japan

Environmental remote sensing and lidar activities at CEReS, Chiba University

Center for Environmental Remote Sensing (CEReS)
Hiroaki Kuze
千葉大学 環境リモートセンシング研究センター
久世宏明

The 2nd International Workshop on Vegetation Lidar and Application from space
第2回 衛星搭載植生ライダーとその応用に関する国際ワークショップ 2017年5月26日（金）

CEReS : Center for Environmental Remote Sensing
千葉大学 環境リモートセンシング研究センター

CEReS was established in 1995 to promote cutting-edge researches in Remote Sensing, and apply RS to various environmental problems. Since the 2nd midterm management period starting from 2010, CEReS has been accredited by the MEXT as one of the nation-wide joint usage and joint research centers.

http://www.cr.chiba-u.jp/

CEReS staff and students (April 2016)

Ground-based validation studies and fostering of next-generation researches in both the domestic and international settings

Satellite data and ground-based validation activities

Research topics are closely related to social issues such as climate change, food & water security, disaster mitigation, etc.

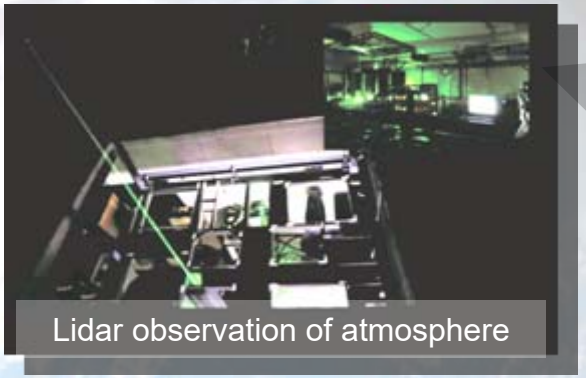

Lidar observation of atmosphere

Studies are ongoing on light propagation in the atmosphere, various active and passive remote sensing techniques, and treatment of satellite data as big data.

Developing MW sensors onboard an UAV

Microwave sensors can detect surface targets even nighttime or cloudy conditions. Our research aims at developing a small satellite with CP-SAR sensors.

A unique RC helicopter system has been developed in the course of studies for better estimation of biomass.

Biomass observation with an RC helicopter

Overseas joint observations

Various joint observations are carried out to understand the exact environmental conditions worldwide.

Observation with drones

Drone-based environmental observation is studied for supporting agriculture and disaster control

Laser measurement of forest

A simulator has been developed to reproduce the reflectance characteristics of forests. Laser instruments are employed to grasp the 3D structure of forest canopies.

Proximity remote sensing based on UAV platform　Prof. A. Kondoh

➢ Remote sensing systems based on UAVs (drone or RC helicopter) can acquire high-resolution images of relatively narrow areas at low cost, with less constraints of place and time.

➢ In FY2013 we conducted the project "Creation of an air dose rate map by low altitude unmanned helicopter measurement and creation of vegetation and land coverage map by using hyperspectral technique" granted by the Ministry of the Environment.

➢ Various sensors on UAV have enabled the low-cost RS applications including air dose rate mapping, crop growth diagnosis, disaster monitoring, temperature and humidity survey, etc.

（Left）Radio-controlled multi-copter,（Right）RS system onboard an engine helicopter.

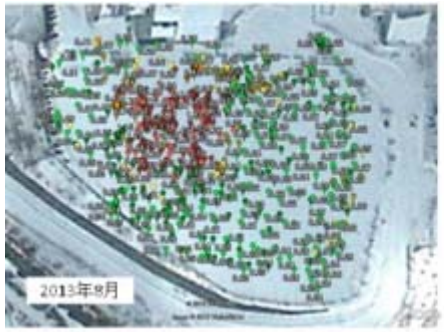

UAV-measured dose rate: red points indicate the temporal storage of contaminated soils.

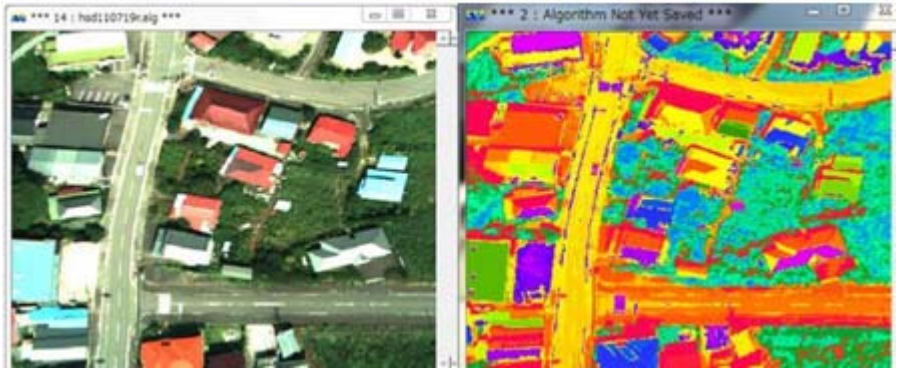

（Left）Aerial photo taken from the UAV,（Right）Hyper-spectral image obtained at low cost.

Disaster monitoring using Synthetic Aperture Radar (SAR) data

Prof. Josaphat Tetuko Sri Sumantyo

➢ Sub cm-order movements due to subsidence, earthquakes, etc., can be detected with the SAR method (DInSAR, PS-InSAR) from JERS-1, ALOS, TerraSAR-X satellite data.

➢ Land subsidence in Jakarta city area was monitored at a resolution of 1 m. The data were used by Indonesian government.

➢ Landslides were mapped in Malay peninsula in a ICA・JST SATREPS program. The government used the data for highway management.

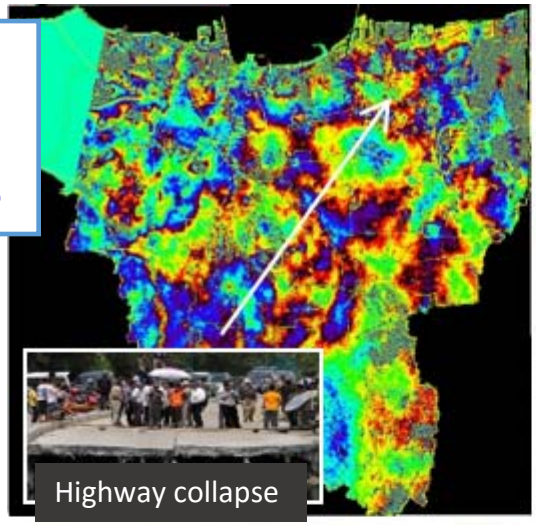

(Left) Subsidence in Jakarta detected in a SAR image (Below) Newspaper reporting the contribution of CEReS.

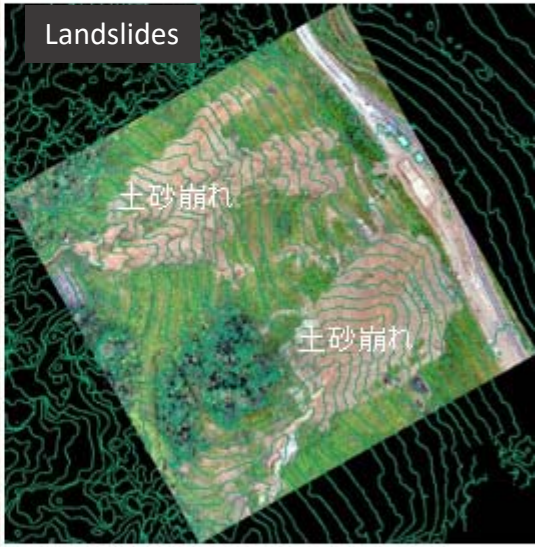

(Left) Mapping landslide sites in Malay peninsula (JICA・JST SATREPS), (Right) Validation at a site along a highway. The change in land height was evaluated.

Disaster monitoring using CP-SAR sensors onboard small satellites

Prof. Josaphat Tetuko Sri Sumantyo

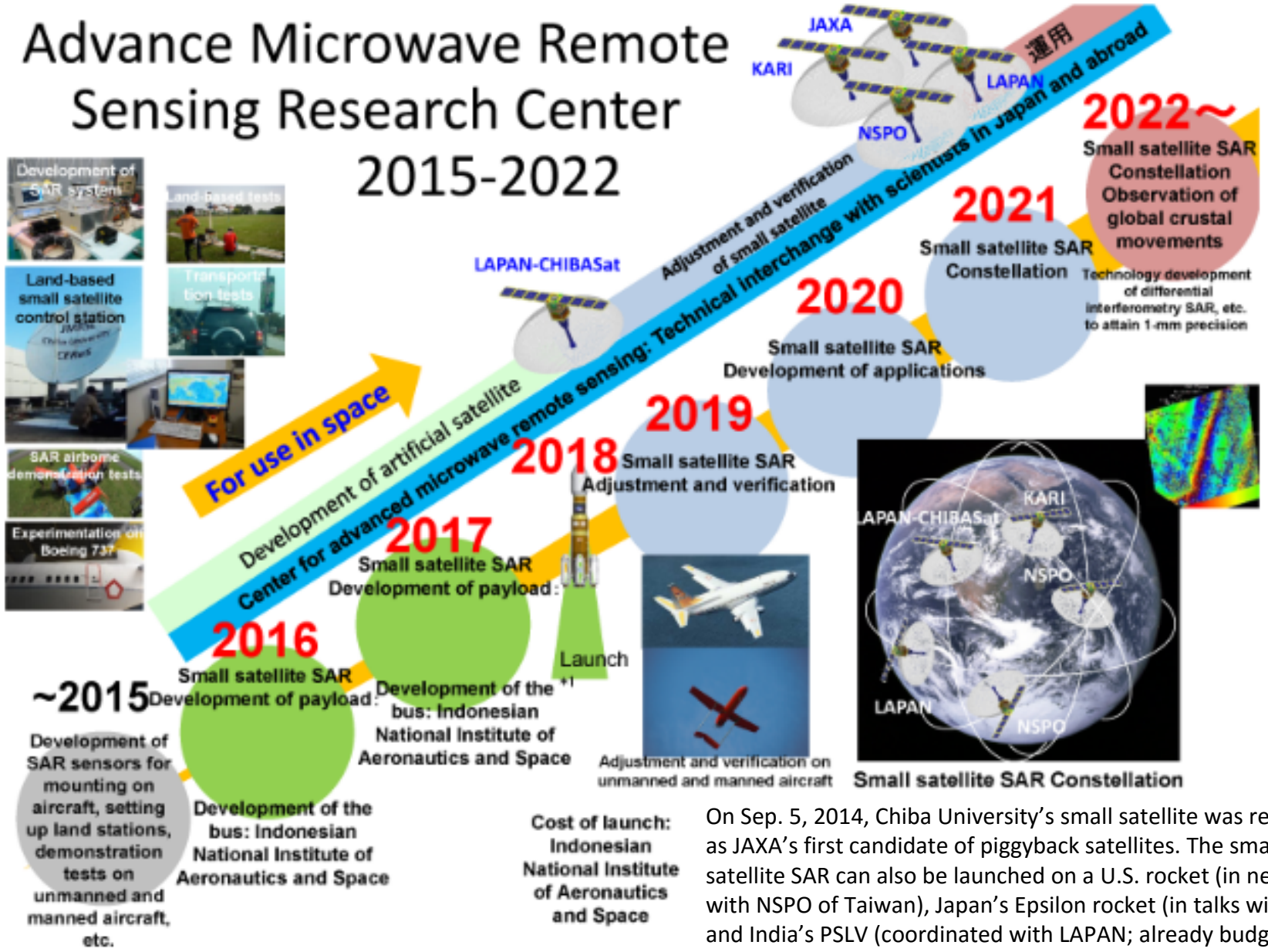

On Sep. 5, 2014, Chiba University's small satellite was registered as JAXA's first candidate of piggyback satellites. The small satellite SAR can also be launched on a U.S. rocket (in negotiation with NSPO of Taiwan), Japan's Epsilon rocket (in talks with IHI) and India's PSLV (coordinated with LAPAN; already budgeted).

Advantage of CP for SAR measurements

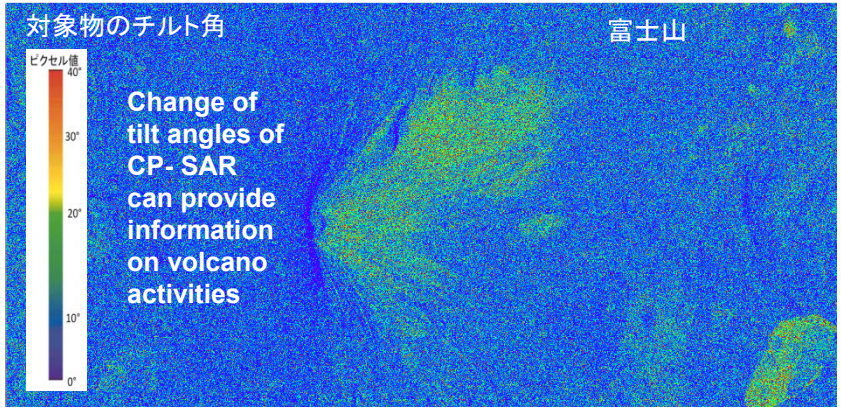

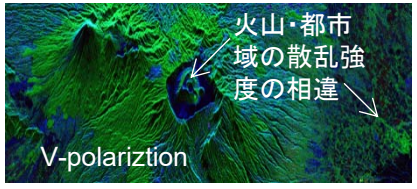

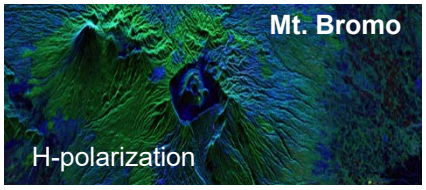

Optical vs. SAR images

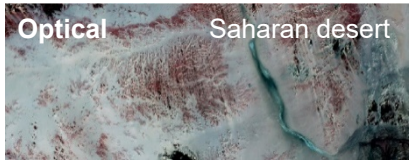

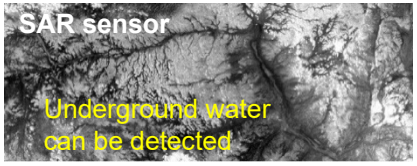

	Explanation
Synthetic Aperture Radar (SAR)	All-weather microwave sensor that can be applied for both day- and night-time scenes. A large aperture antenna is virtually realized by exploiting the movement of the platform (aircraft of satellite), resulting in high spatial resolution (3 m).
CP-SAR	Circularly polarized synthetic aperture radar A novel SAR sensor proposed by Chiba University. Conventional SAR sensors are based on linear polarization, which is significantly affected by the Faraday rotation effect in the ionosphere. This effect is considered to be much smaller in the case of CP: moreover new parameter can be used for better characterization of the target.

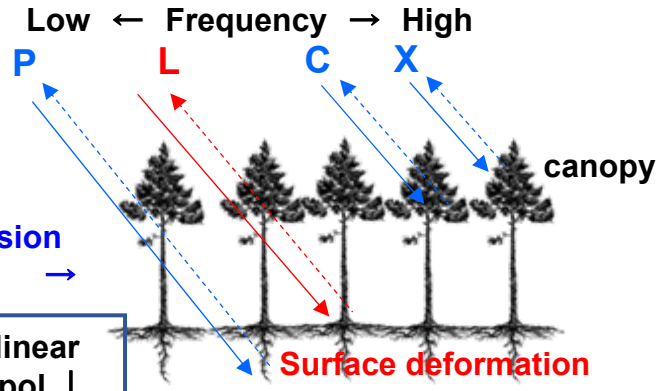

L-band (1.27 GHz) is most suitable for land surface monitoring
Difference in transmission →

Comparison between linear (LP) and circular (CP) pol. ↓

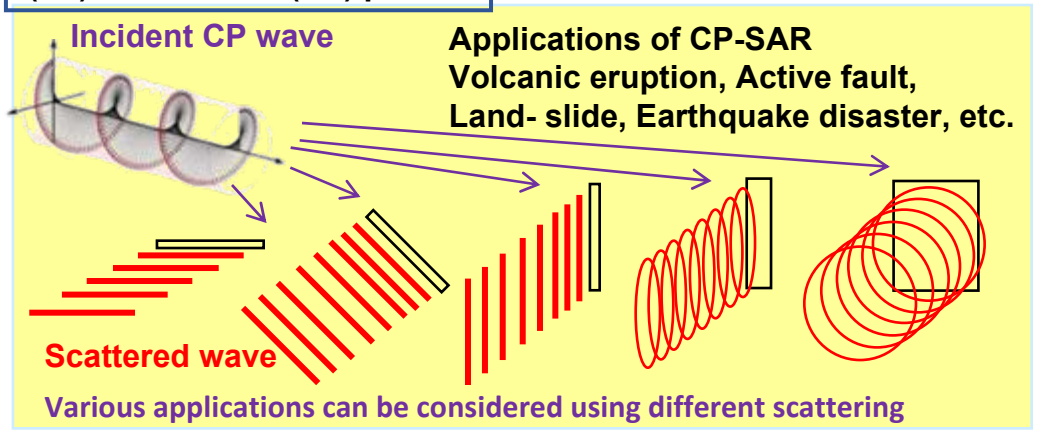

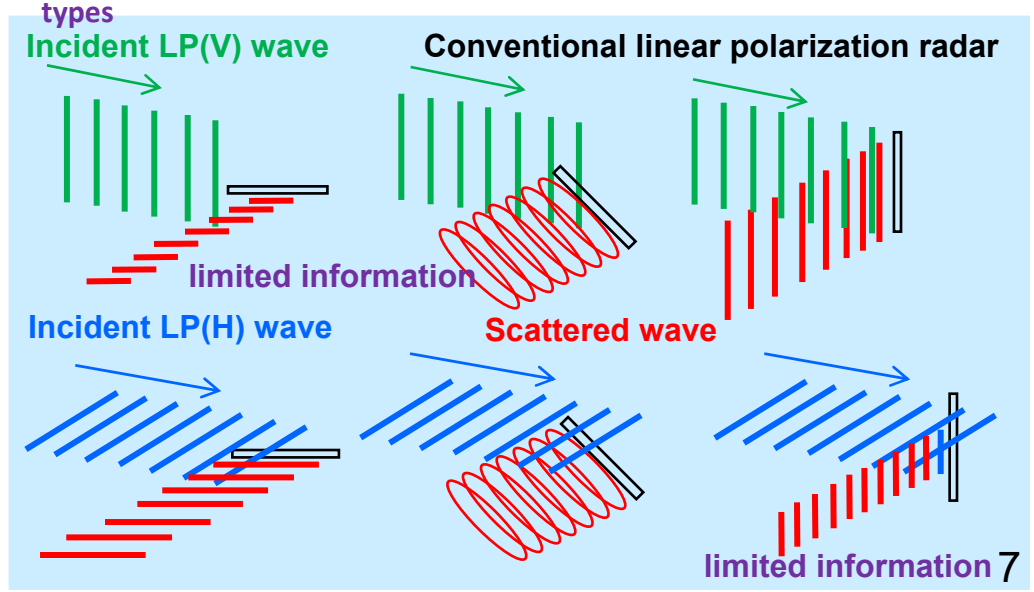

Forecast service on "pollen scattering forecast based on satellite data"

Prof. Chiharu Hongo

➢ **Amount of wind blown pollen can be predicted from weather data, number of male flowers and MODIS / fPAR (photosynthetic effective radiation absorption rate) data.**

➢ **The team of CEReS and Weathernews Co. has started a new pollen forecasting service, which is a valuable service for hay fever patients and businesses producing hay fever related products.**

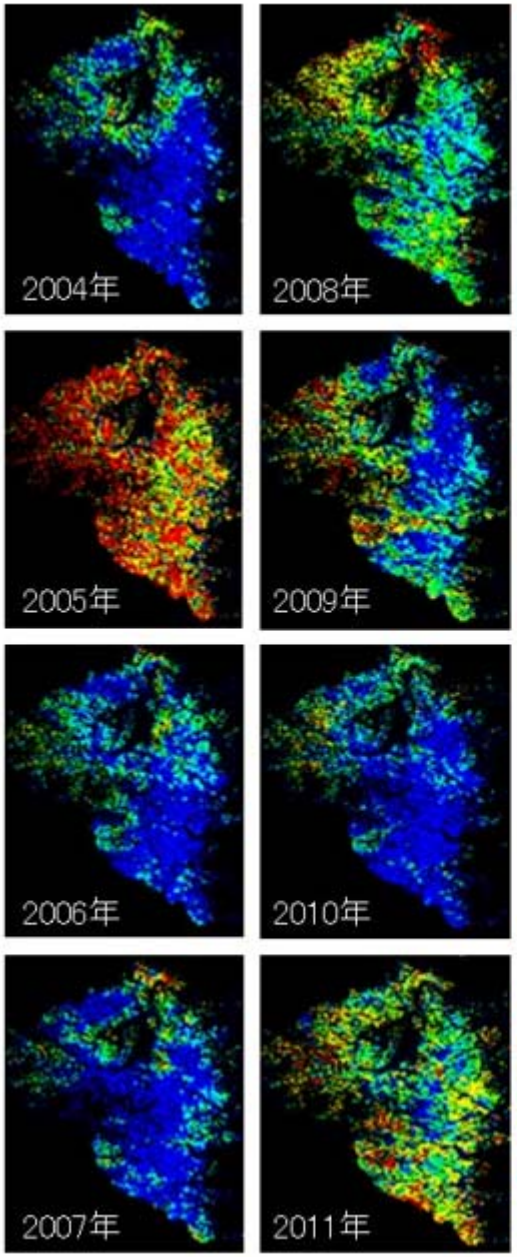

Comparing 2015/2014

Forest activity map

High activities of coniferous trees
⇒ More male flowers
⇒ More pollen scattering in Saitama, Tokyo, and Chiba Prefectures

2016-2021 Science and Technology Research Partnership for Sustainable Development (SATREPS) Prof. Chiharu Hongo

➢ (Title)

Development and Implementation of New Damage Assessment Process in Agricultural Insurance as Adaptation to Climate Change for Food Security

➢ (Overseas Partner)

Indonesian government,
Bogor Agricultural University

➢ (Abstract)

This project aims to establish new method of damage assessment in order to effectively implement the assessment, the core of agricultural insurance system, for Indonesia which has started trial projects as adaptation to climate change.

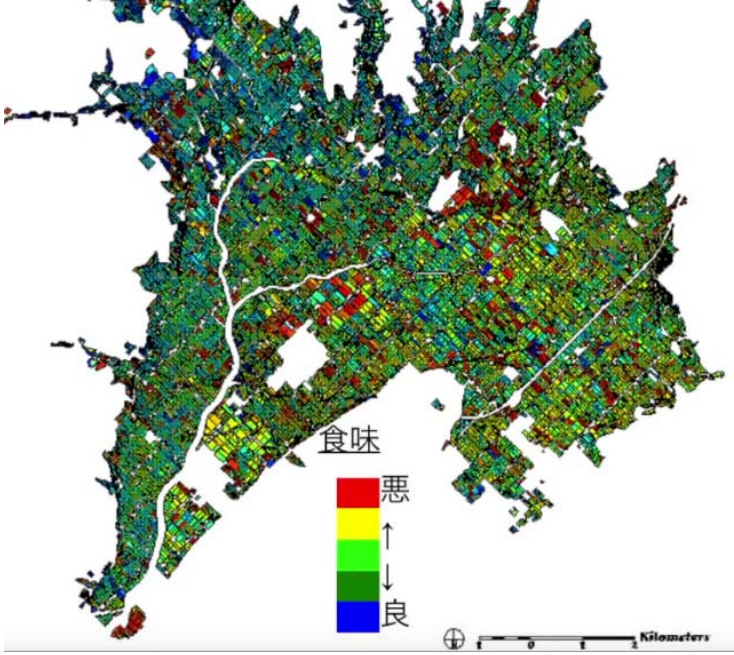

(1) To establish an effective method covering wide area to assess paddy rice damage by drought, flood and pest and disease, making full use of satellite & UAV data, GIS and ground survey data.

(2) To integrate current and new assessment methods, with implement-tation of new methods.

(3) To construct information infra- structure needed for operation and improvement of damage assessment methods.

(4) Capacity development for the establish-ment and operation of damage assessment methods.

New method for measuring average concentration of CO_2 in the urban atmosphere

Prof. Hiroaki Kuze

➢ **This research demonstrated the capability of measuring long-term changes in CO_2 concentration by transmitting 1.5 μm radiation generated from a wide-band light source for optical communications.**

➢ **The use of high resolution (0.046 nm) spectrometer has enabled the simultaneous measurement of CO_2, H_2O, and HDO concentrations.**

➢ **The method is particularly useful for urban environment where the measurement of regionally averaged concentrations is often hindered by the presence of many local sources.**

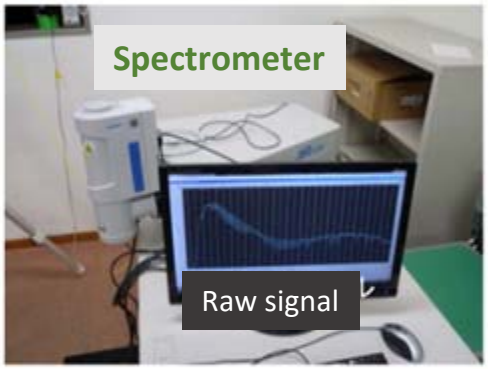

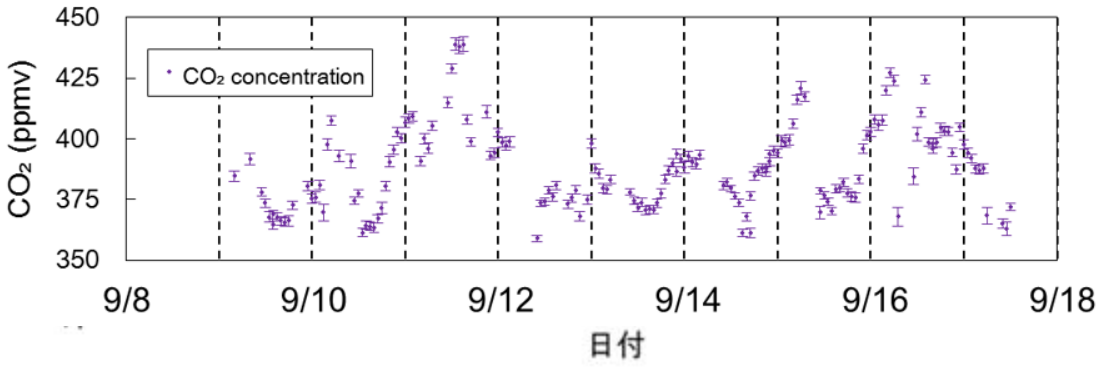

The collimated IR beam was sent toward a retro-reflector placed at a rooftop of a building 2.55 km apart, and the return beam was detected using a receiver telescope connected to a high-resolution spectrometer.

NO_2 pollution in the East Asia - back to the level of 5 years ago

Prof. Hitoshi Irie

➢ **OMI satellite data** was validated by means of RS based on the **MAX-DOAS** method. Subsequently, the analysis of OMI data has led to the estimation of **NO_2 column amount** over each country.

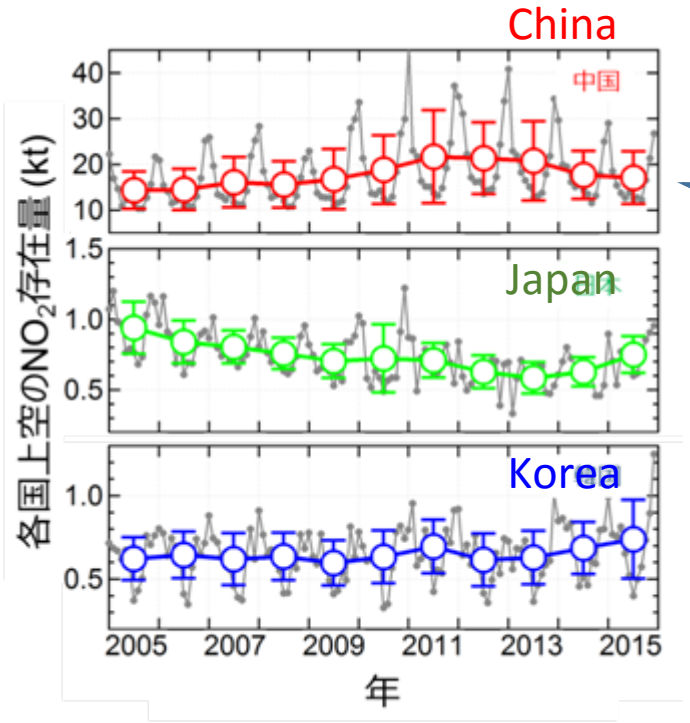

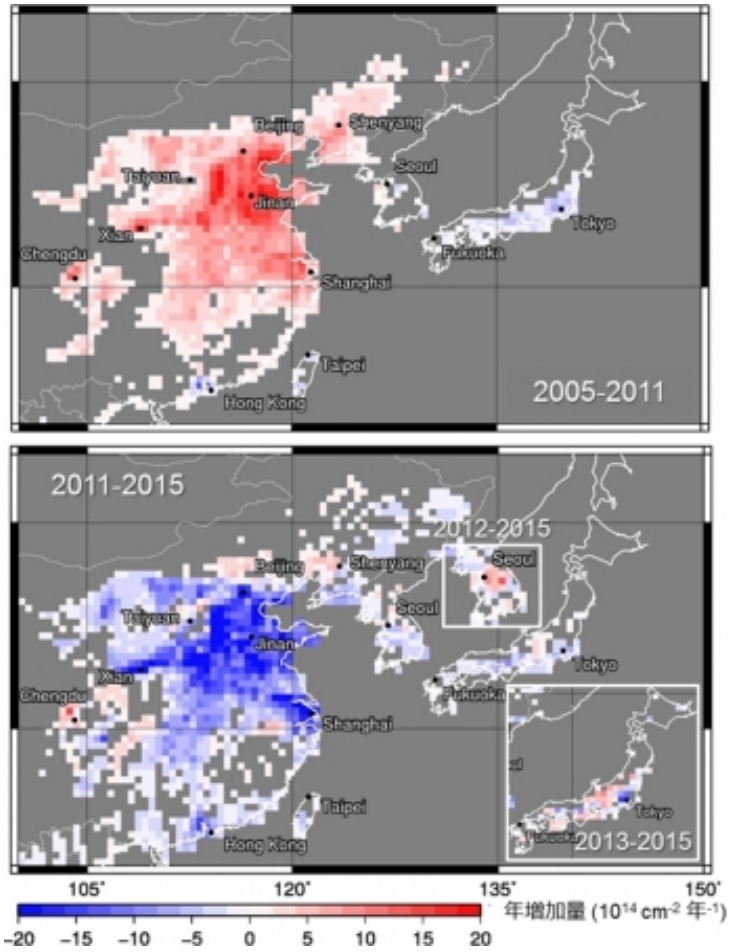

Increasing annual trend until 2011

Decreasing annual trend after 2011

➢ **During 2011～2015, annual decreasing trend of 6%/year was observed over China. This is considered to be the effect of air pollution control such as the spread of denitrification equipment.**

➢ **A slight deterioration trend o NO_2 pollution was seen over Japan after 2013.**

GCOM-C: Global estimation of biomass

Prof. Y. Honda & Prof. K. Kajiwara

➢ Long-term observation of 10 – 15 years will be made globally in the Global Change Observation Mission to elucidate global climate change and water circulation mechanism.

➢An autonomously piloted RC helicopter was developed in the Mongolian grassland observation campaign conducted in 1990s.

➢ Subsequently, it was shown that multi-angle observations of forest canopy can lead to the precise estimation of the above ground biomass (AGB).

Observation of Mongolian grassland

➢ Similar capability of multi-directional observation will be implemented in the new GCOM-C satellite mission. CEReS and JAXA team will analyze and validate the global data.

➢ The understanding of the Earth's ecosystem through GCOM-C will greatly contribute to enhance the sustainability of human society.

Auto-pilot RC helicopter for remote sensing

Integration of site observation, RS data, and models toward better understanding of terrestrial carbon cycles

Prof. Kazuhito Ichii

Keywords:
Terrestrial Biosphere, Carbon Cycle
Remote Sensing, Model, Machine Learning
Synthesis

➢ **Upscaling of terrestrial CO_2 fluxes using site data, RS data, and machine learning**

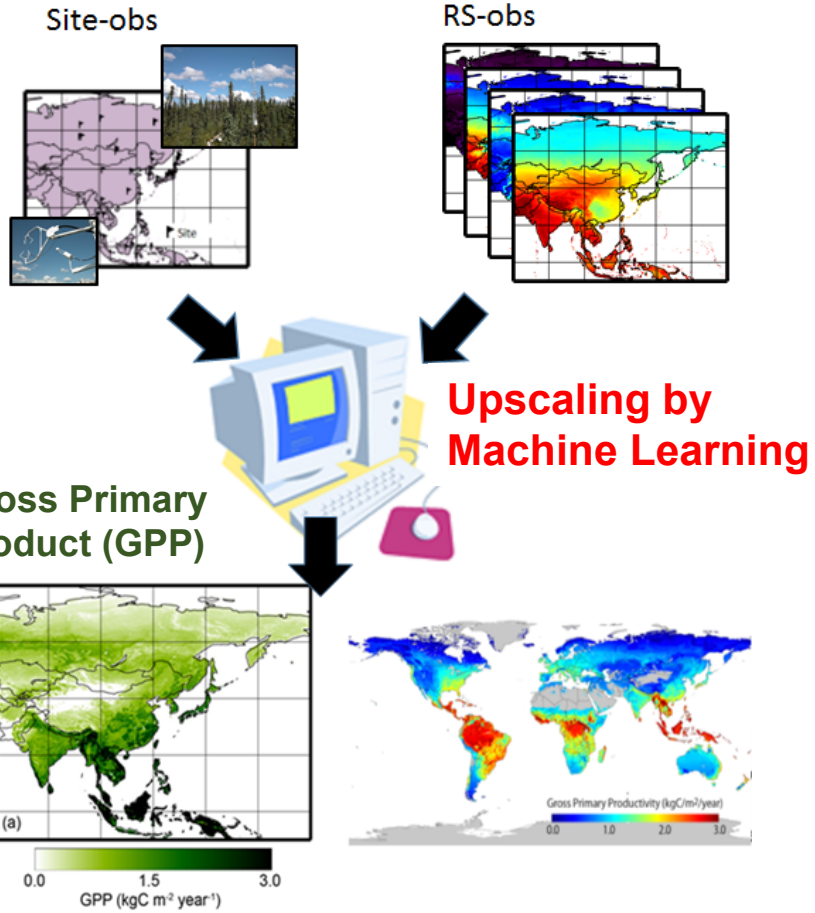

[Ichii et al. 2017] [Kondo et al. 2015]

➢ **Refinement of terrestrial ecosystem model using RS-based products (model-data integration)**

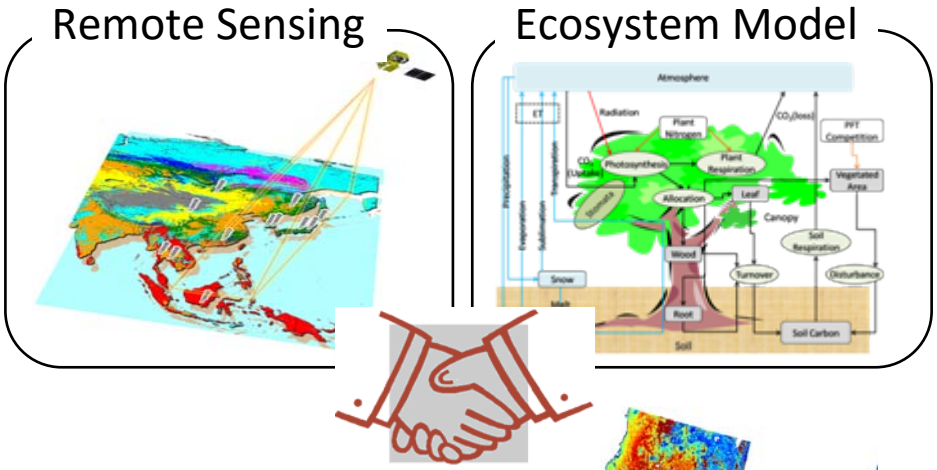

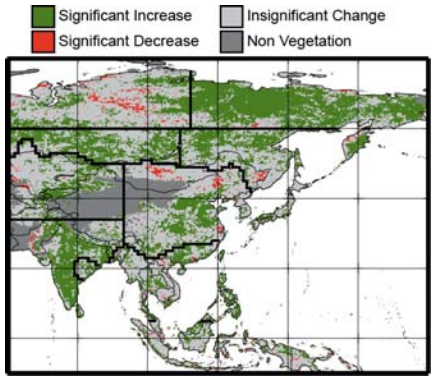

Vegetation Change in Asia [Ichii et al. 2013]

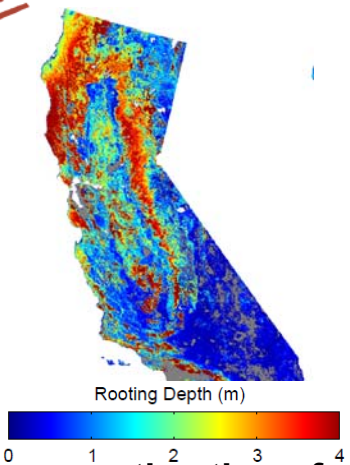

Inverse estimation of root depth [Ichii et al. 2009]

CEReS archive system for Himawari-8 : The 3rd generation geostationary meteorological satellite

Prof. Atsushi Higuchi

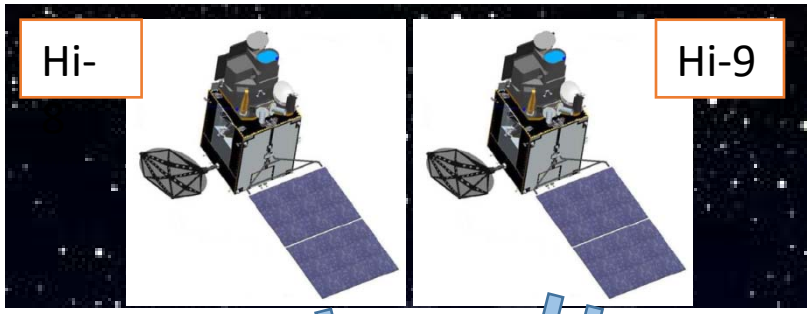

36,000 km above the equator

HOPE (気象衛星ひまわり運用事業) Himawari Operation Enterprise Corp.

Private optical fiber connection

JAXA
U. Tokyo

Met. Satellite Center (Kiyose)

Japan Meteorological Agency

Routine weather forecast

CEReS, Chiba University

Large scale data archiving system

Providing facilities for data processing
- Generation and dissemination of gridded data and higher level products

Internet

Practical use, e.g. local governments

Overseas use

Research community

New phase environmental research

Release of Himawari-8 precision gridded data **Prof. Atsushi Higuchi**

http://www.cr.chiba-u.jp/databases/GEO/H8_9/FD/

Standard full disk data

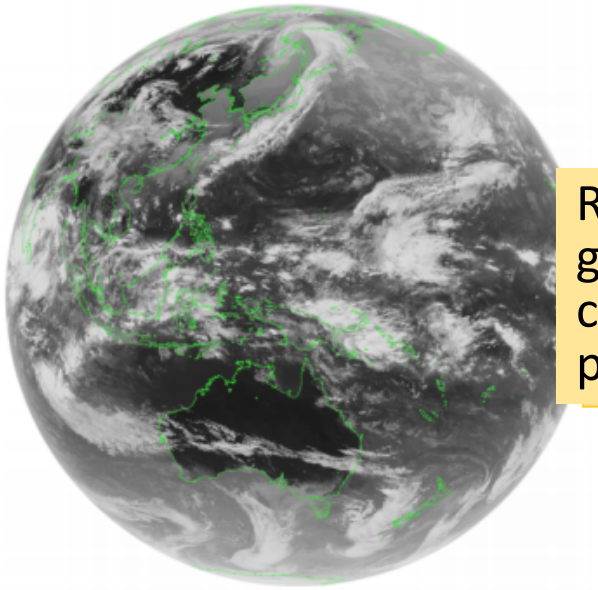

Real-time geometric correction using parallel computing

Gridded data

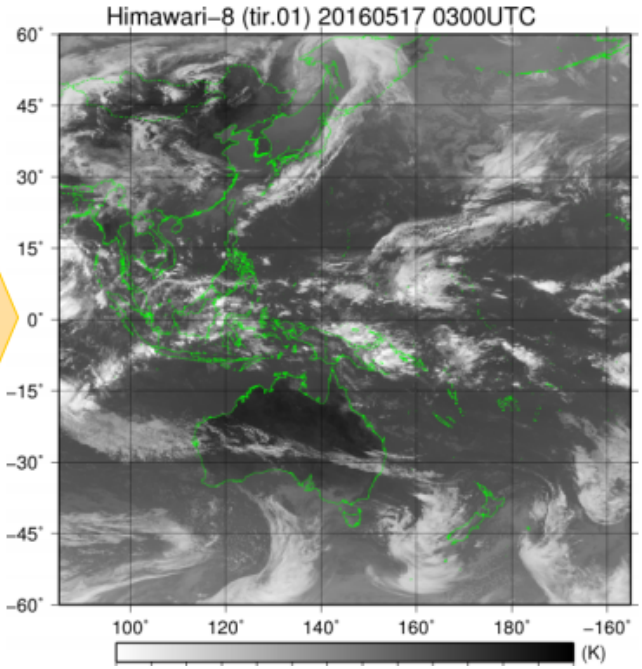

*No coastline information is included in original Himawari-8 data.

➢ **Himawari-8 data has officially been used since July 2015. Significant improvements have been made for resolution, observation bands (5 to 16), and observation frequency (60 min to 10 min for full disk mode).**

➢ **The standard data are provided in full disk. CEReS has developed a fast processing system that has enabled the transformation to gridded data within 40 s (data volume for 1 month is 3 TB for all the 16 bands).**

Canopy level fluorescence detection Kuze Gr.

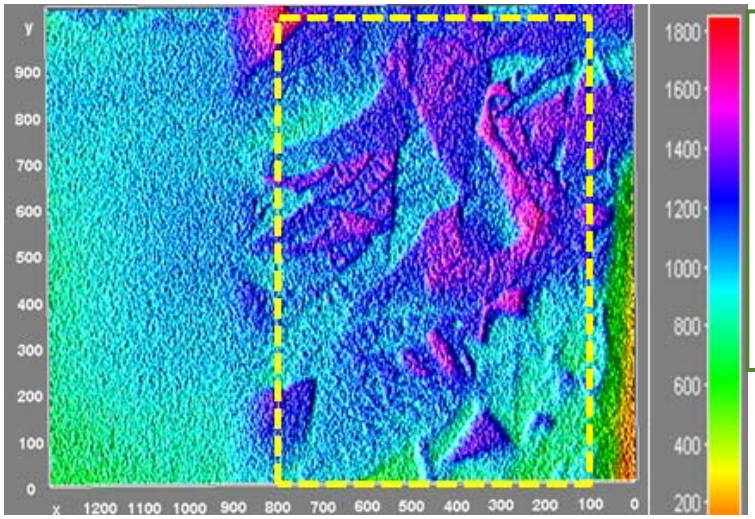

Average SIF intensity per pixel is calculated from a region of 700 ×1000 pixels

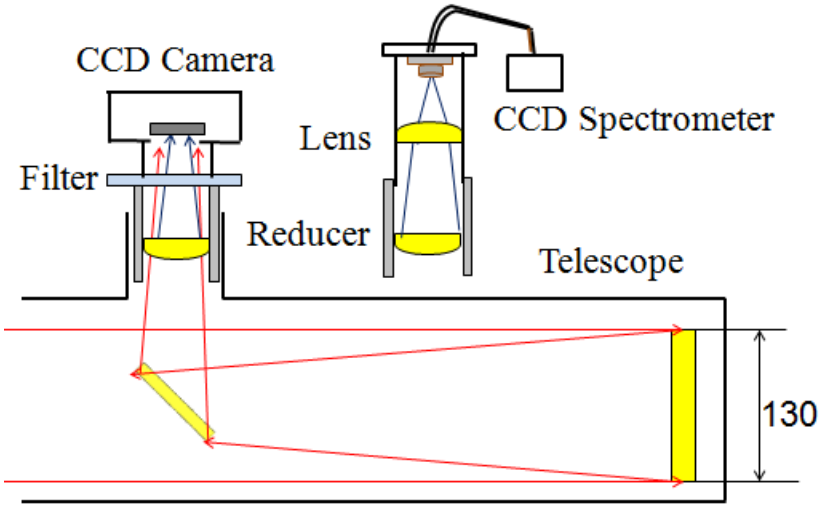

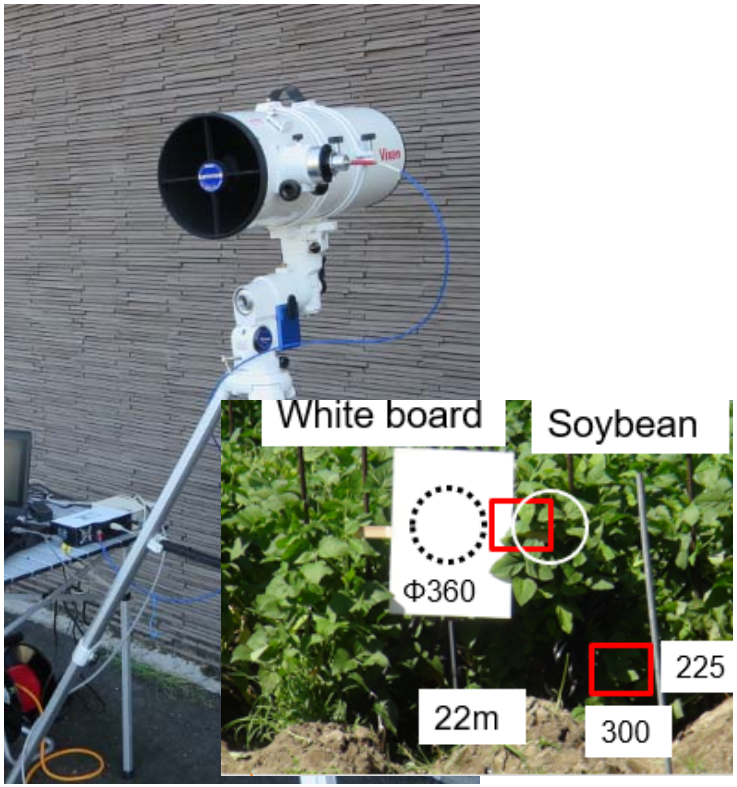

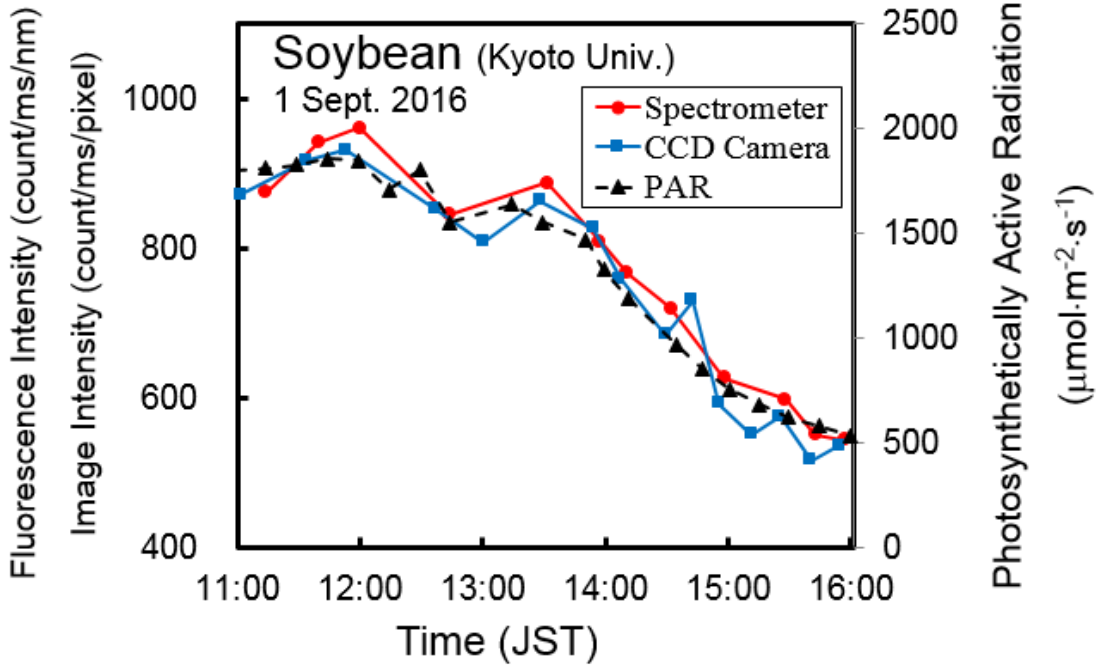

Lidar monitoring of atmospheric aerosol
ライダーによる大気エアロゾル観測

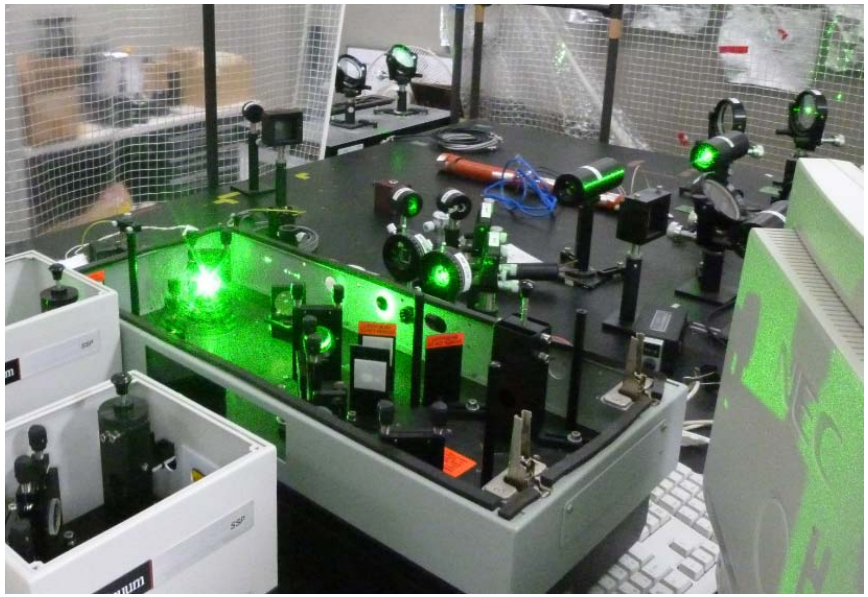

Multi-wavelength lidar observation of tropospheric aerosols

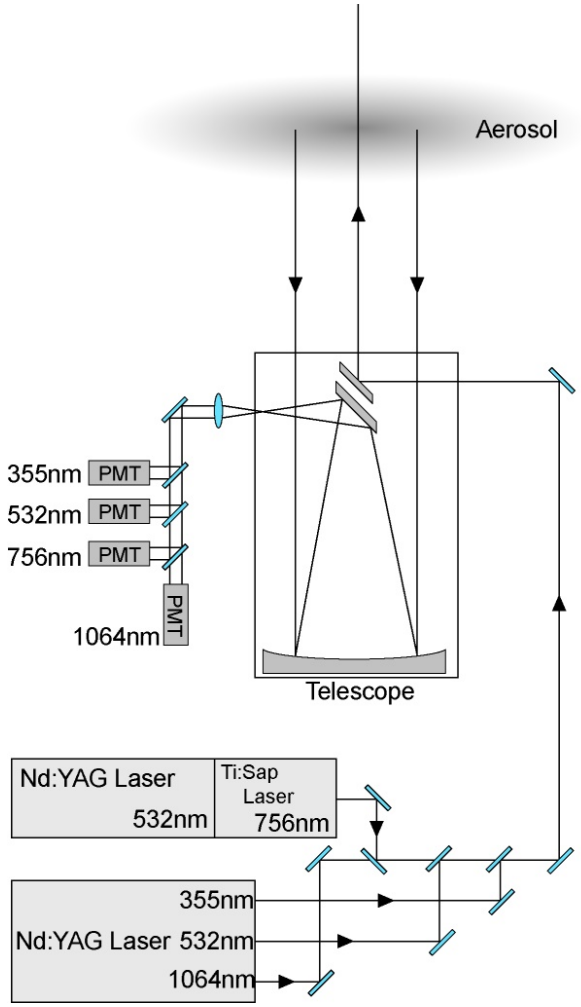

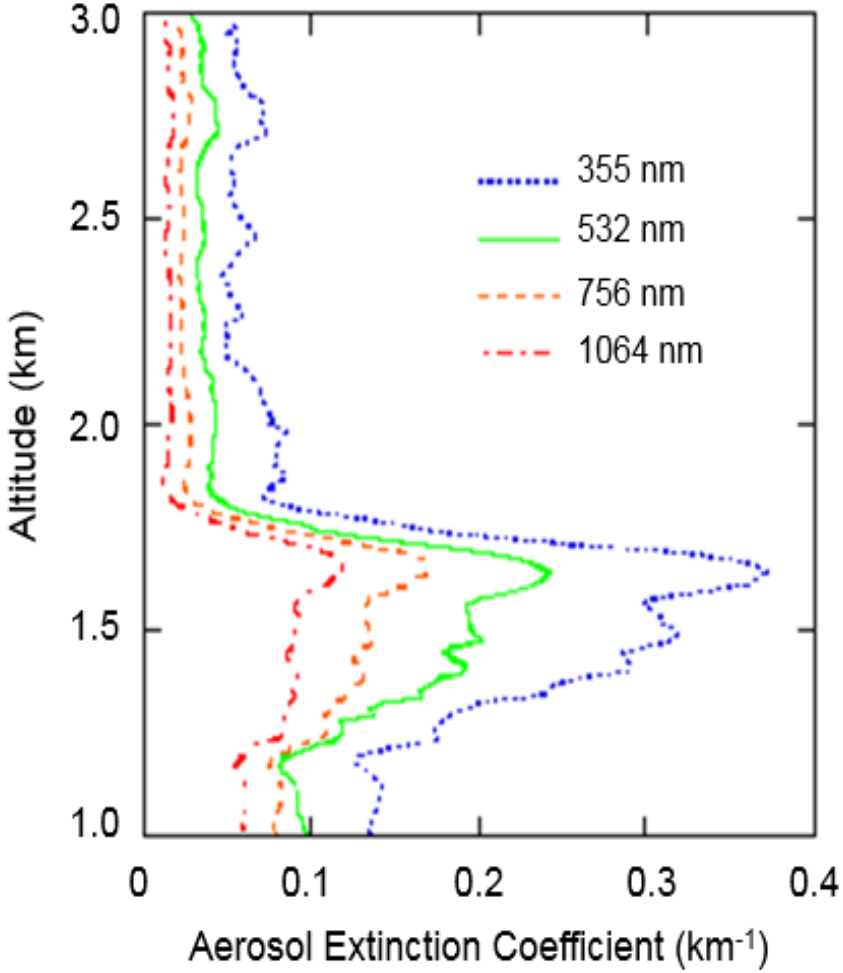

➢ エアロゾルの粒径分布を含めた高度分布情報が取得できる。ただし、遠方での信号校正とライダー比 S_1 の正確な評価が前提となる。Information on aerosol size distribution can be retrieved for each altitude, though precise and comprehensive calibration is needed for quantitative analysis of lidar data.

ライダー方程式（空気分子とエアロゾル）
Two-component Lidar Equation (backscattering)

total optical thickness (τ)

$$P(R) = P_0 \frac{c\tau}{2} AK \frac{G(R)}{R^2} \beta(R) \exp\left[-2\int_0^R \alpha(R')\,dR'\right]$$

R target range [m]
$P(R)$ detected power
P_0 emitted power

$\beta(R)$ backscattering coefficient [$m^{-1}sr^{-1}$]
$\alpha(R)$ extinction coefficient [m^{-1}]

Both aerosol and molecular components are considered for α and β.

c speed of light [m/s]
τ laser pulse duration [s]

A telescope area [m^2]
K optical efficiency
$G(R)$ overlapping function

Solution of the lidar equation (Fernald method)

lidar ratio $S_1 = 10 \sim 100$ sr

molecular lidar ratio

$$S_1(R) = \alpha_1(R) / \beta_1(R) = \sigma_1(R) / \left(\frac{d\sigma_1}{d\Omega} \right)_{\theta=\pi}, \quad S_2(R) = \alpha_2(R) / \beta_2(R) = 8.52 \text{ sr}$$

$$\alpha_1(R) = -\frac{S_1(R)}{S_2}\alpha_2(R) + \frac{S_1(R)\, X(R) \exp I(R)}{\frac{X(R_c)}{\frac{\alpha_1(R_c)}{S_1(R_c)} + \frac{\alpha_2(R_c)}{S_2}}} + J(R)$$

R_c : far-end boundary

$$X(R) = R^2 P(R), \quad I(R) = 2\int_R^{R_c} \left[\frac{S_1(R')}{S_2} - 1 \right] \alpha_2(R')\, dR'$$

$X(R)$: range corrected signal

$$J(R) = 2\int_R^{R_c} S_1(R')\, X(R') \exp I(R')\, dR'$$

Look-up table (LUT) method

- **Size distribution** [*R. Jaenicke*, 1993]

  $s\,(u)$: u = 0 to 10

  Logarithmic division of the Urban and Maritime aerosol models

- **Complex refractive index**

  real part $m\,(j_1)$: j_1 = 0 to 21

  1.40 — 1.60 (0.01)

  imaginary part $k\,(j_2)$: j_2 = 0 to 300

  0.0000 — 0.0300 (0.0001)

- **Wavelength** $\lambda\,(\ell)$: ℓ =1 to 4

  355, 532, 756, 1064 nm

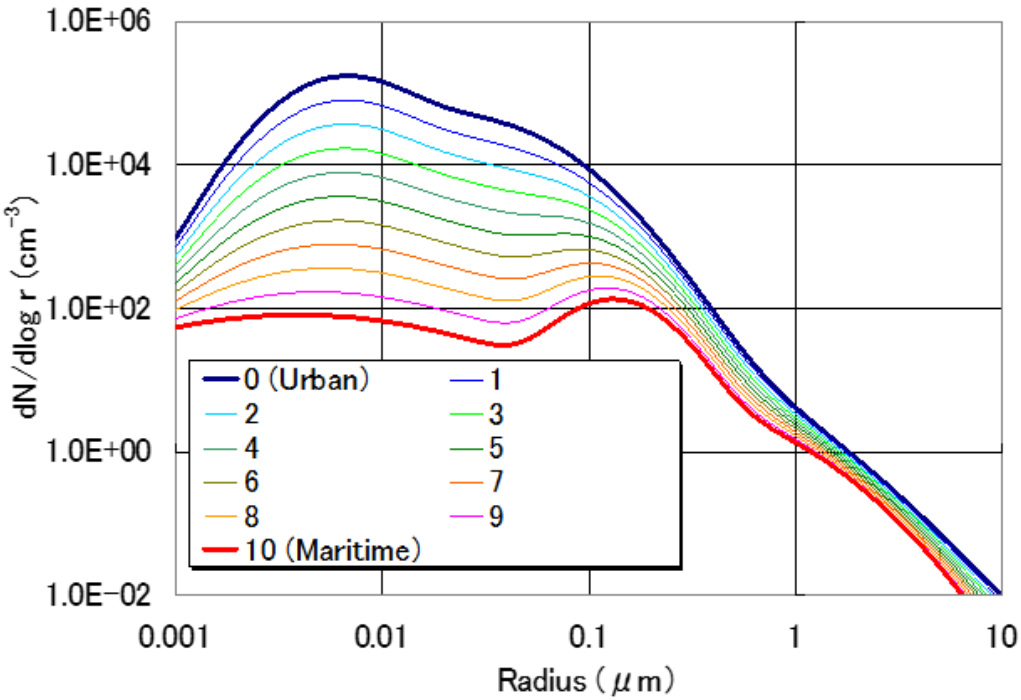

$S_1^{(LUT)}(\ell, j_1, j_2, u)$: S_1 parameter

$\alpha_1^{(LUT)}(\ell, j_1, j_2, u)$: Extinction coefficient

都市型と海洋型のエアロゾルモデル粒径分布をもとに中間的な粒径分布を仮定

Aerosol size distribution for LUT. s =0 corresponds to the urban model, and s =10 to the maritime model.

Vertical profiles of the complex refractive index and size distribution as derived from actual lidar data 多波長ライダーデータから導出した屈折率と粒径分布の高度プロファイル

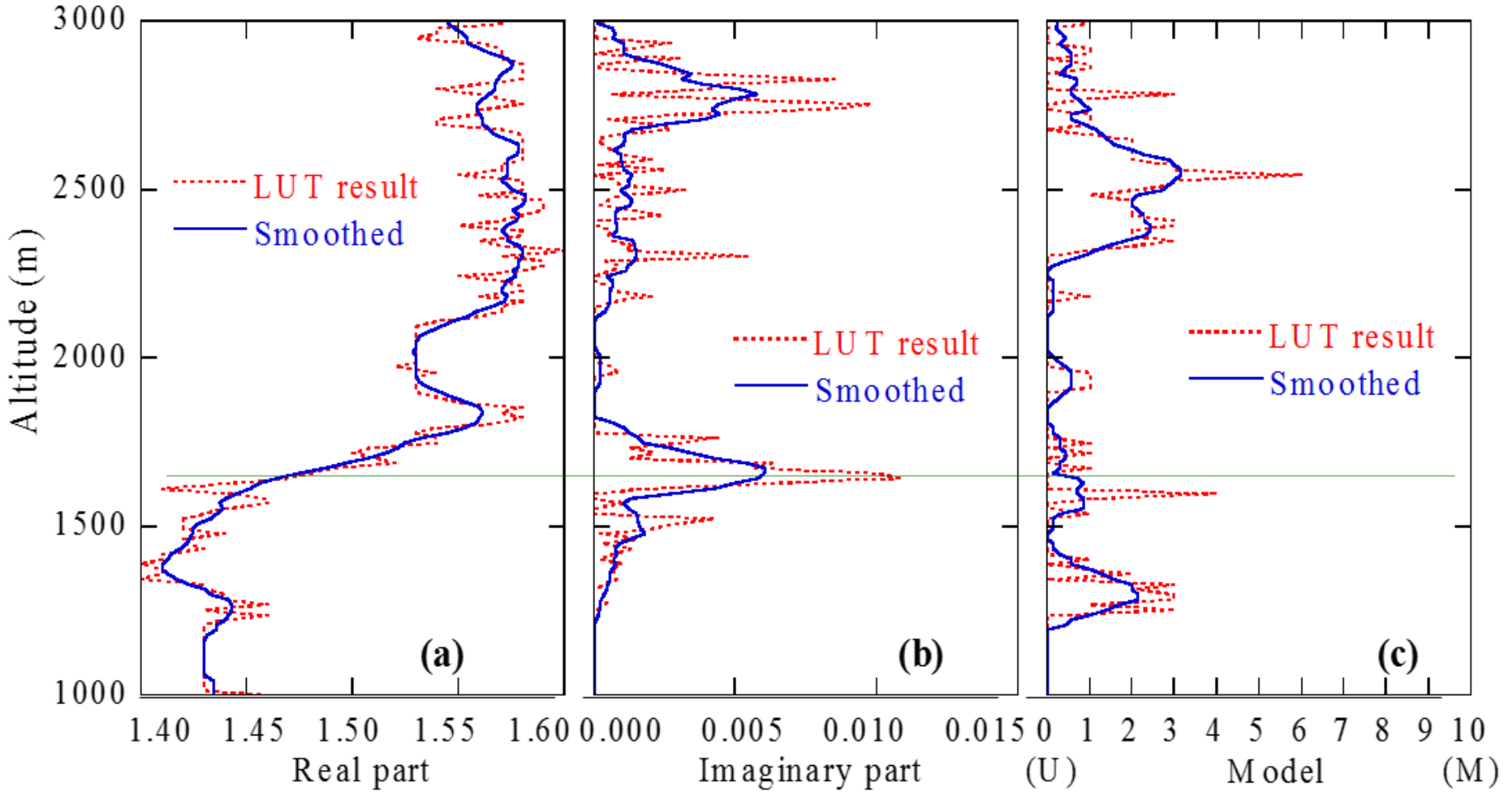

Real part **Imaginary part** **Size distribution model**

M. Yabuki, H. Kuze, H. Kinjo, N. Takeuchi, Jpn.J.Appl.Phys. 42 (2003)

Variation of Angstrom exponent with RH 相対湿度変化とAngstrom指

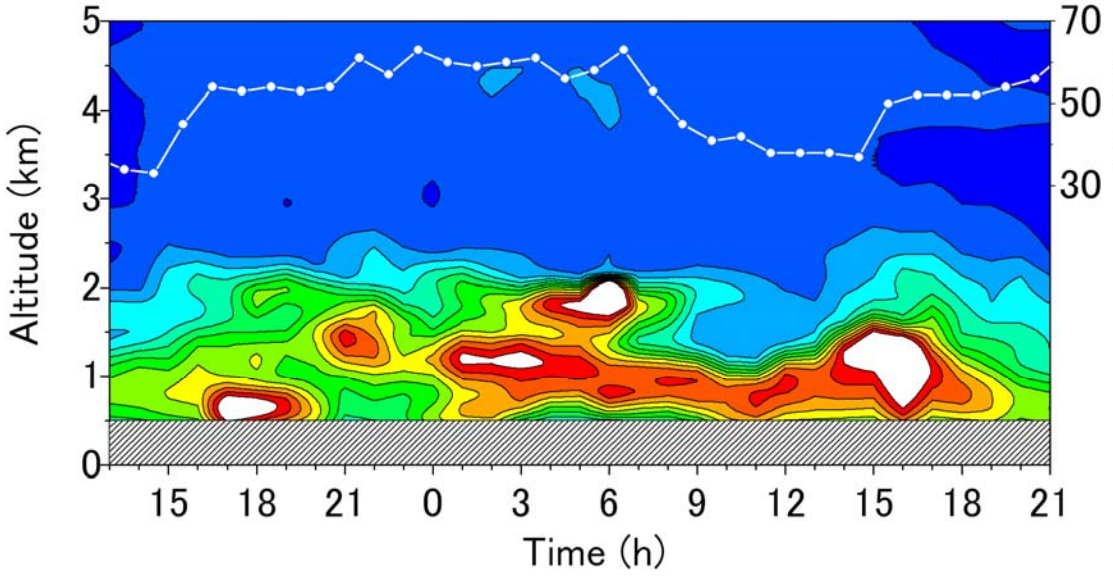

Extinction profile

λ = 1064 nm

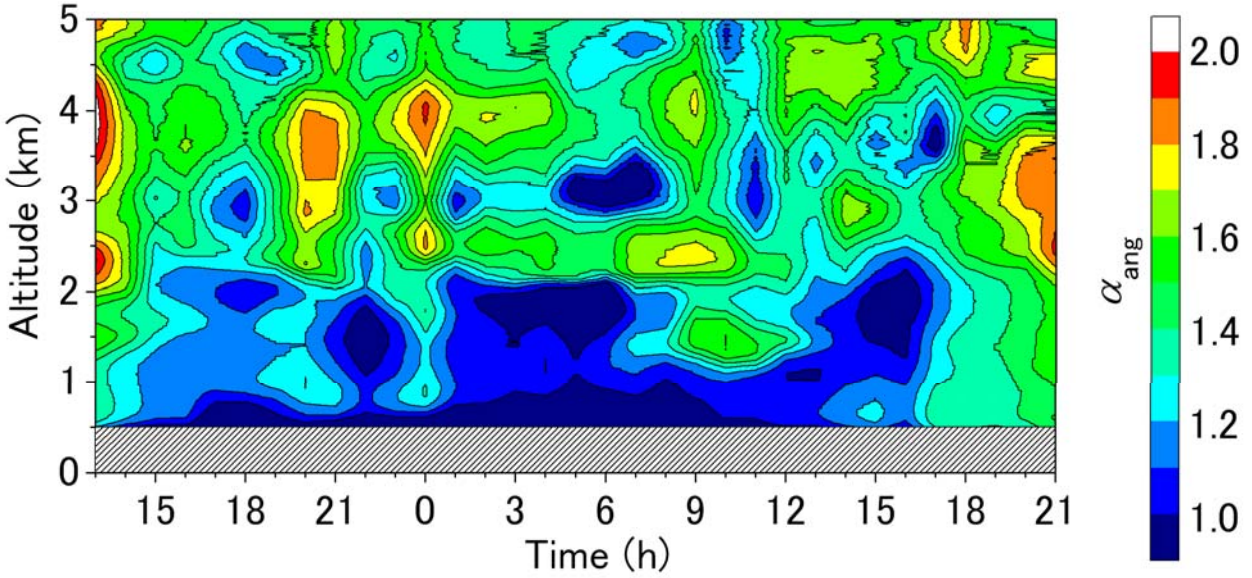

Angstrom exponent derived from α_{ext} at 355, 532, 756 and 1064 nm.

Analysis:

Fernald method

S_1 = 54.7, 53.0, 46.0 and 43.2 sr for each lidar wavelength

(Chiba winter from sampling result)

z_{ref} = 5500 m

Autonomous observation of aerosol & cloud using a portable lidar

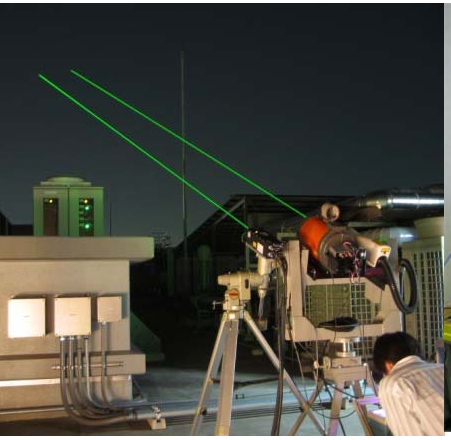

➢ **Portable automated lidar (PAL) system was developed in collaboration with Hamamatsu Photonics Laboratory. 浜松ホトニクスと共同してPALを開発・運用**

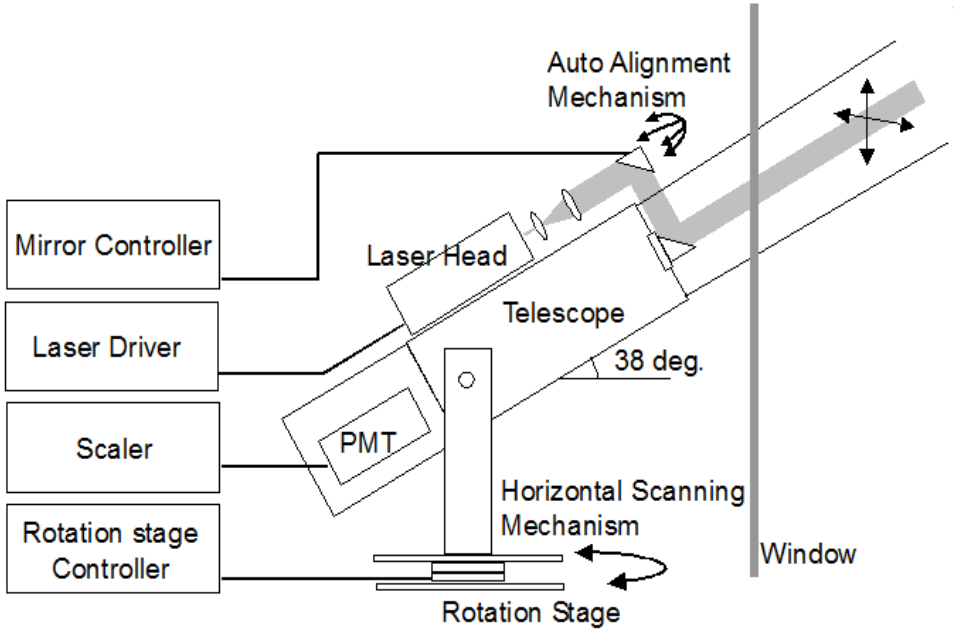

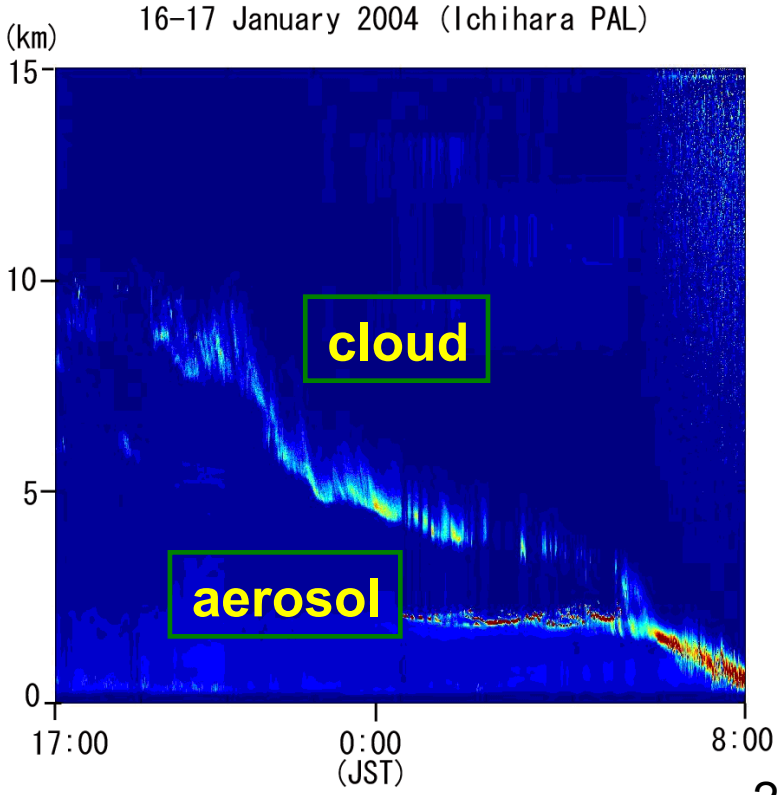

➢ **Automatic alignment was made every 15 min. 自動アラインメント機能**

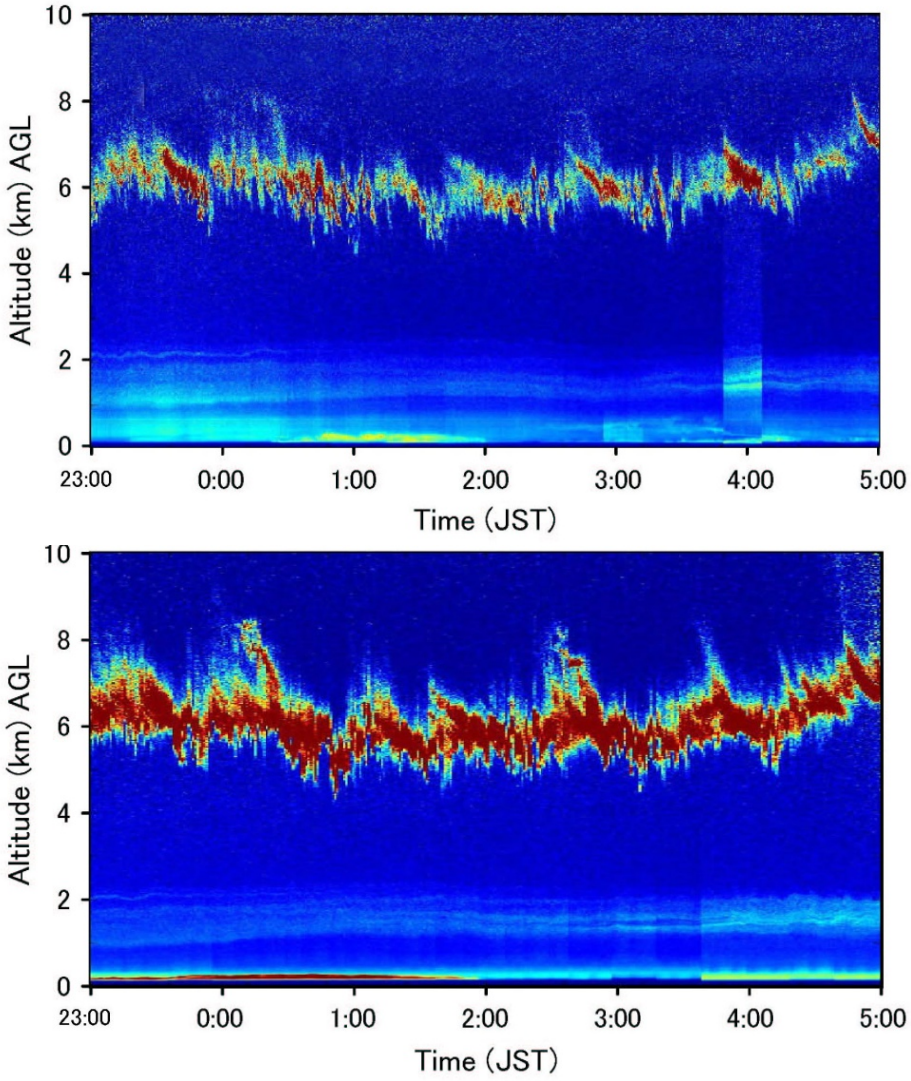

(a) CEReS and (b) Ichihara PAL data, 23:00 of 2 June to 5:00 JST of 3 June 2004

Aerosol plume observed over the Anagawa crossing 081113

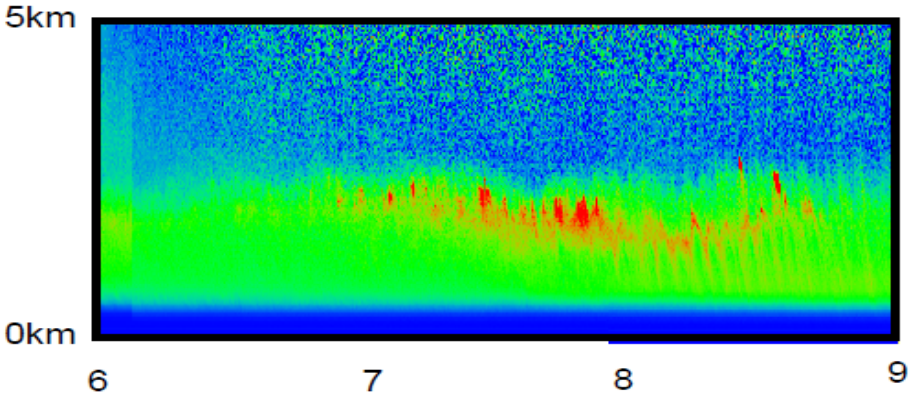

G. Bagtasa, C. Liu, N. Takeuchi, H. Kuze, S. Naito, A. Sone, H. Kan, Opt. Rev. 14 (2007)

Bistatic imaging lidar observation of aerosol and cloud

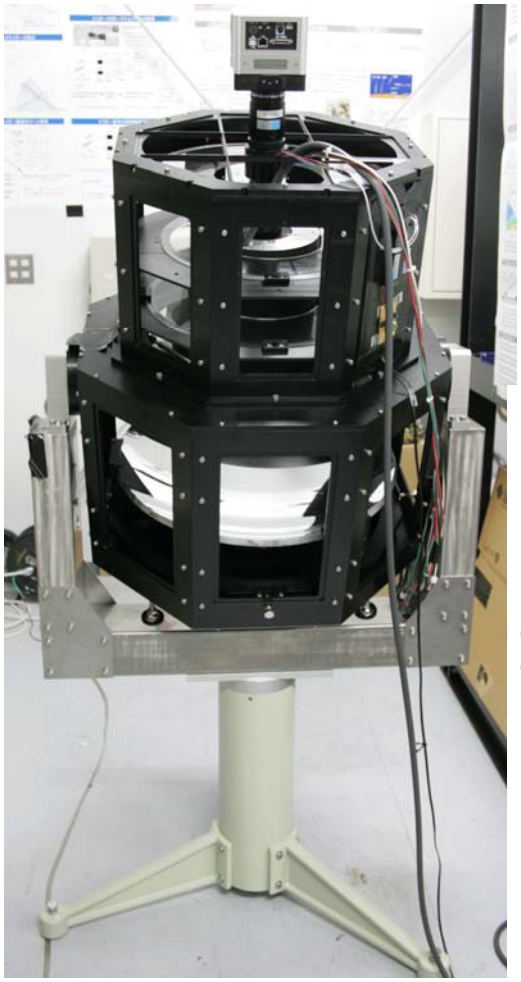

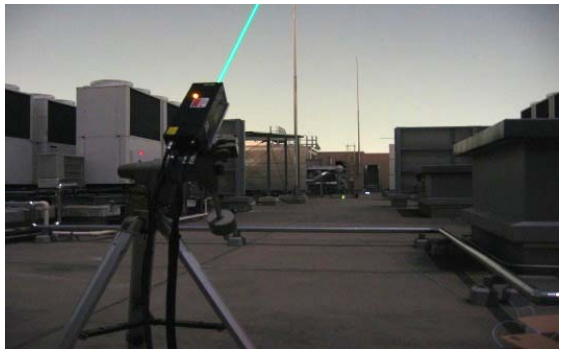

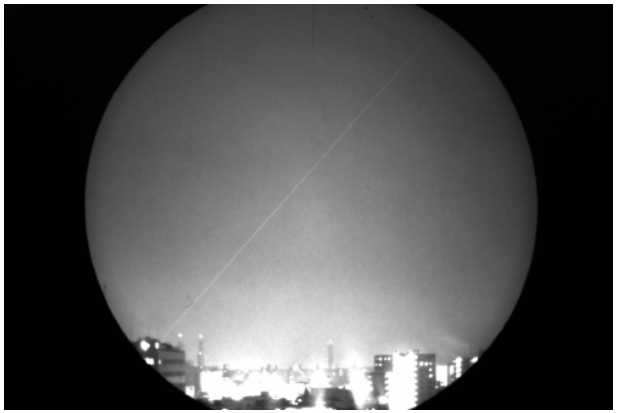

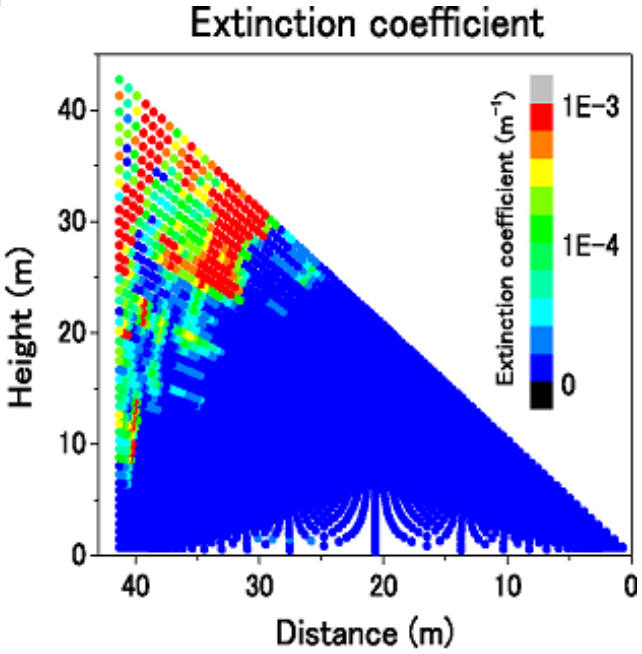

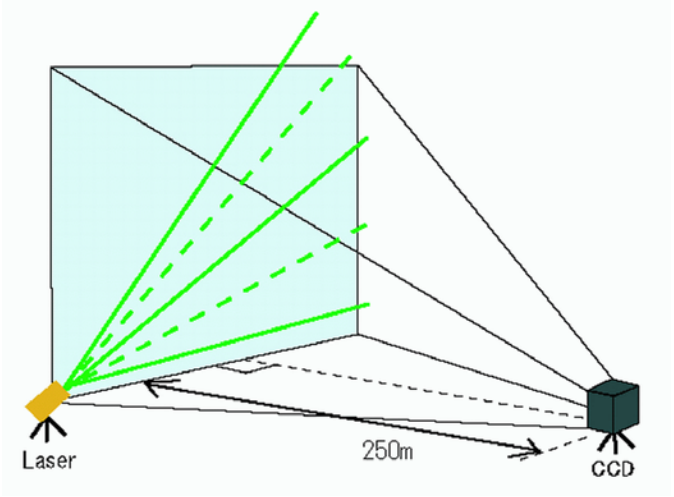

An imaging lidar was developed using the Ashra (All-sky Survey High Resolution Air-shower) telescope framework in collaboration with the Institute for Cosmic Ray Research, the University of Tokyo.

Bistatic Lidar Equation

$$P = P_0 \; K \; \frac{A}{r^2} \; ds \; \beta(\theta_{\text{scat}}) \; T$$

P	received signal intensity [W]
P_0	emitted laser intensity [W]
K	the efficiency of the receiving optics
A	telescope mirror area [m^2]
r	the distance between the target and telescope [m]
ds	the portion of laser beam path subtended by the FOV for a single pixel of the array detector [m]
β	scattering coefficient [m^{-1}sr^{-1}]
α	extinction coefficient [m^{-1}]
θ_{FOV}	FOV for a single pixel [deg]
θ_{scat}	scattering angle [deg]
f	phase function
τ_t	optical thickness of the transmitter side
τ_r	optical thickness of the receiver side

Subscript 1 is for aerosol and 2 for air molecule

Advantage of bistatic configuration

Since ds is proportional r, the net dependence on r is $1/r$, not $1/r^2$

⇒ low dynamic-range requirements

$$\beta(\theta_{\text{scat}}) = \alpha_1 \; f_1(\theta_{\text{scat}}) + \alpha_2 \; f_2(\theta_{\text{scat}})$$

$$T = \exp\left[-(\tau_t + \tau_r)\right]$$

$$ds = \frac{r \; \theta_{\text{FOV}}}{\sin(\theta_{\text{scat}})}$$

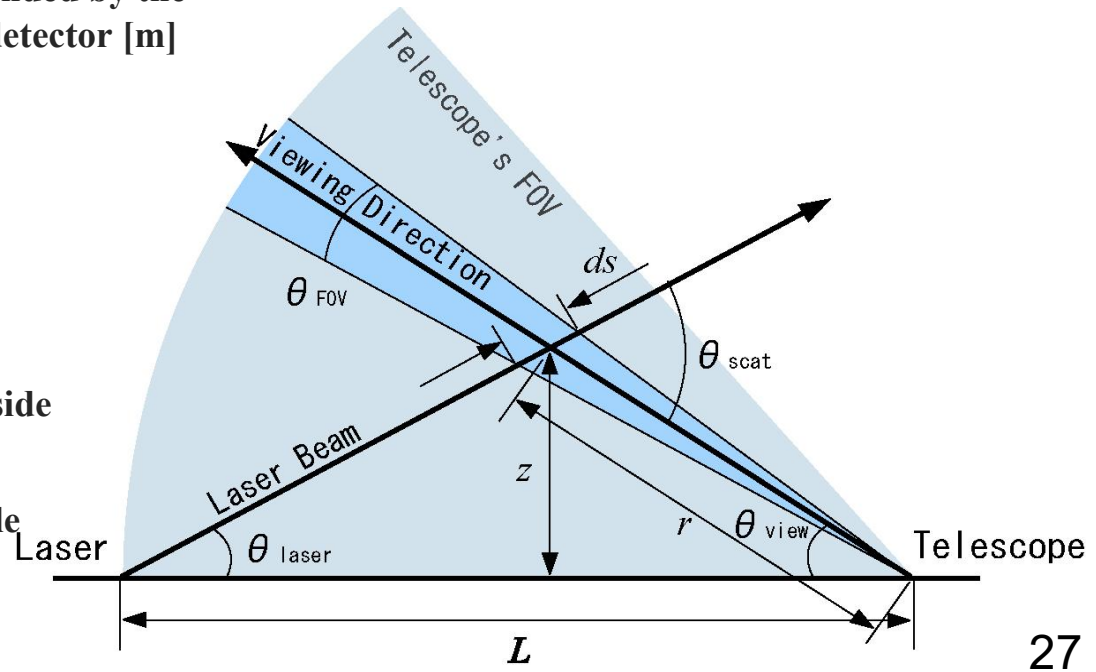

Schematic of 1/3-scale model Ashra telescope

Wavelength range is designed in the UV range of 300-420 nm.

FOV : 31 deg

Angular resolution : 4.3 arcmin (1.26 mrad)

1/3-scale Ashra telescope

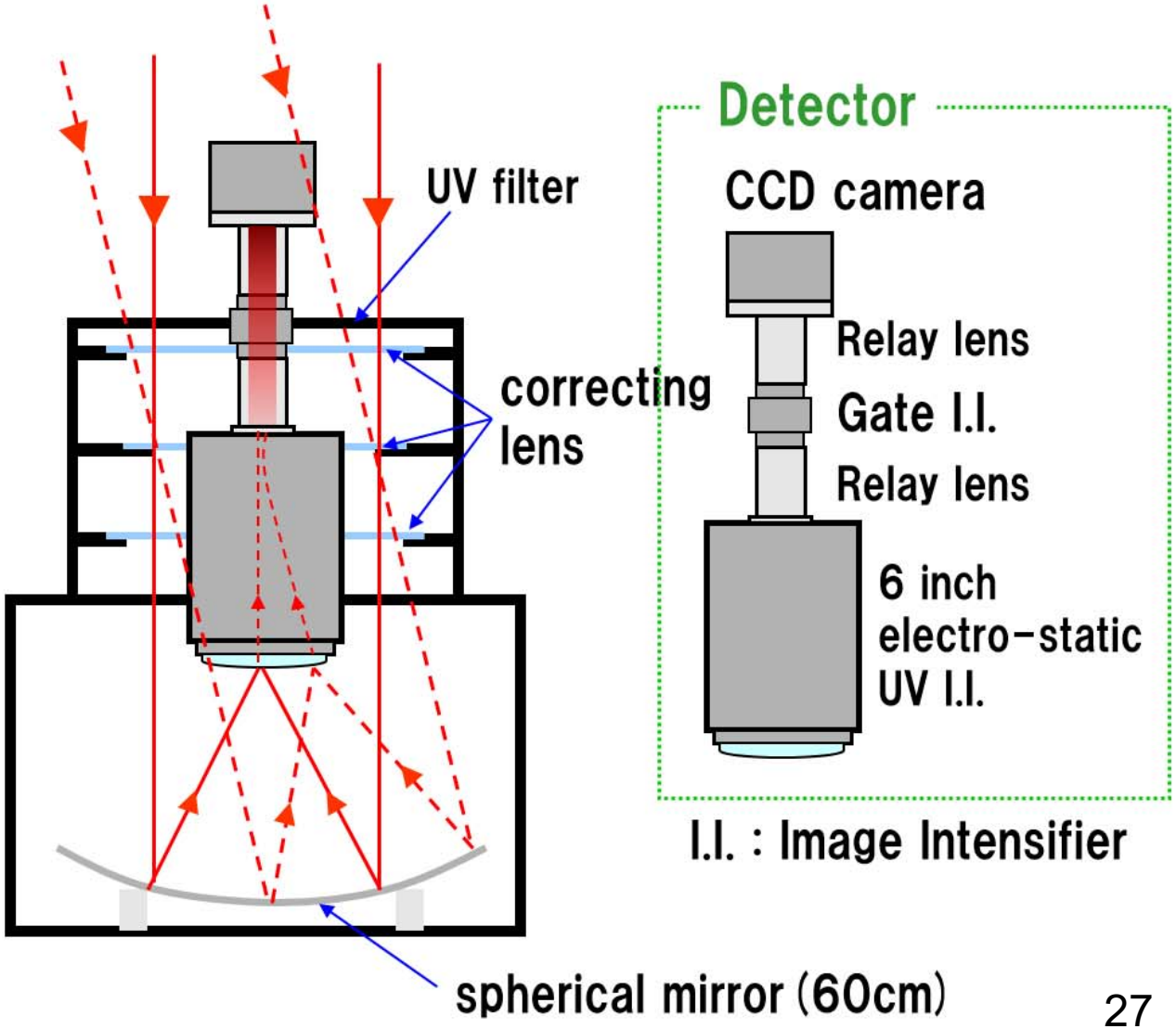

Changing elevations angles and comparison with simulation

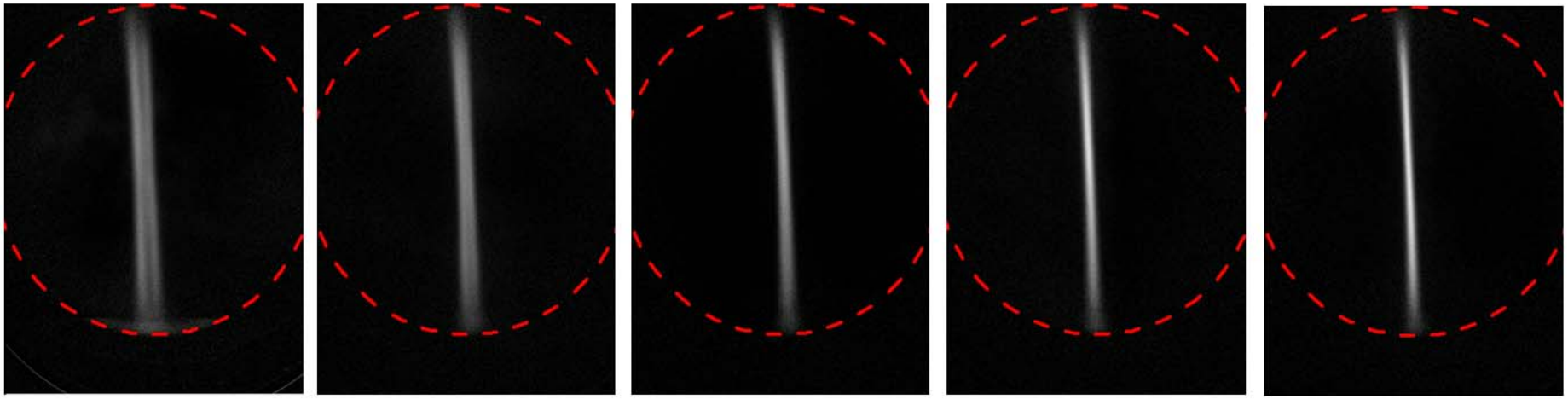

30 deg　40 deg　50 deg　60 deg　70 deg

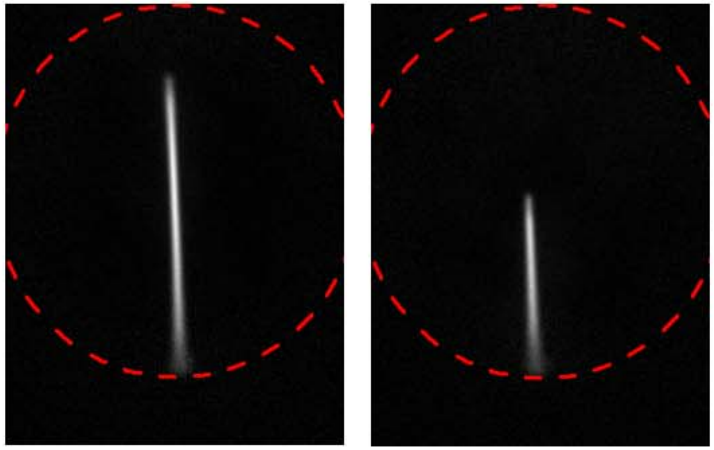

80 deg　90 deg

Scale of difference images : DN 0 ~ 20000

Elevation-angle θ_{laser} : 30~90 deg

Received signal intensity by simulation

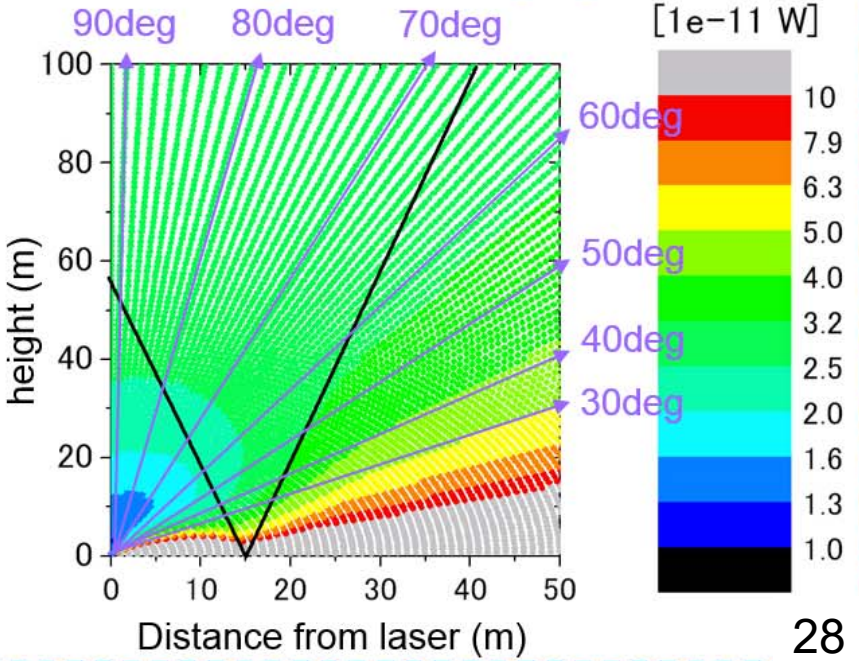

Multi-wavelength lidar unit

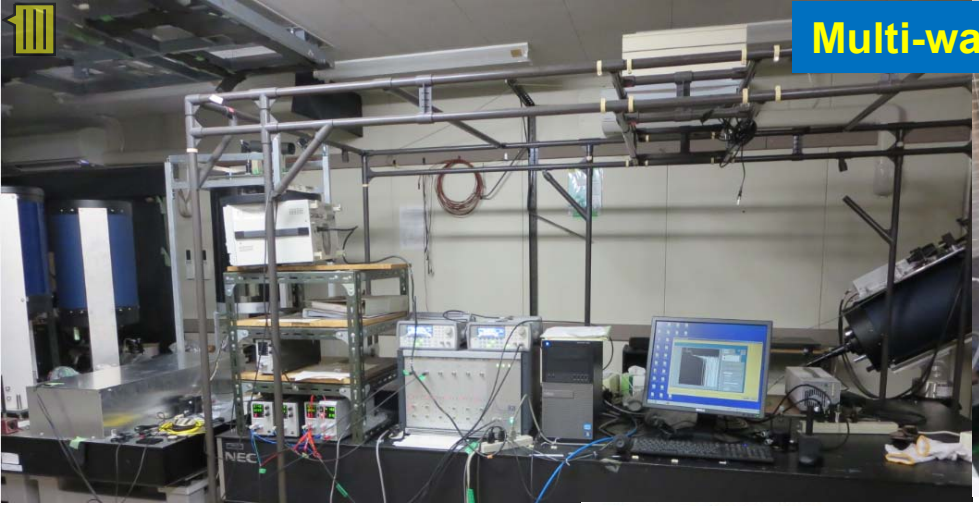

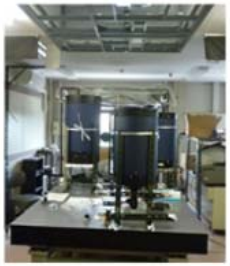

Multi-wavelength lidar unit

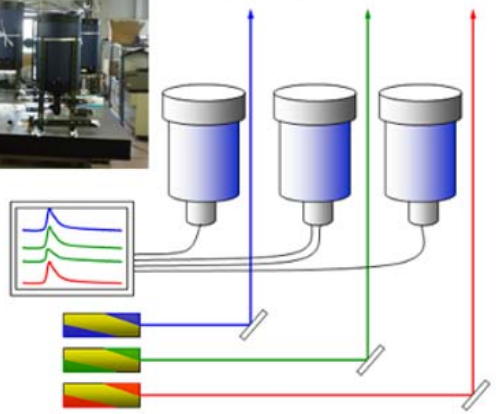

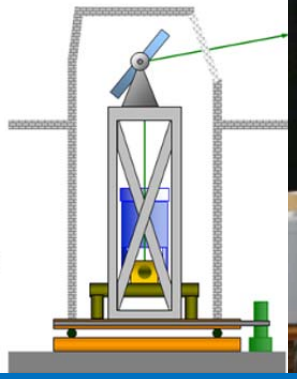

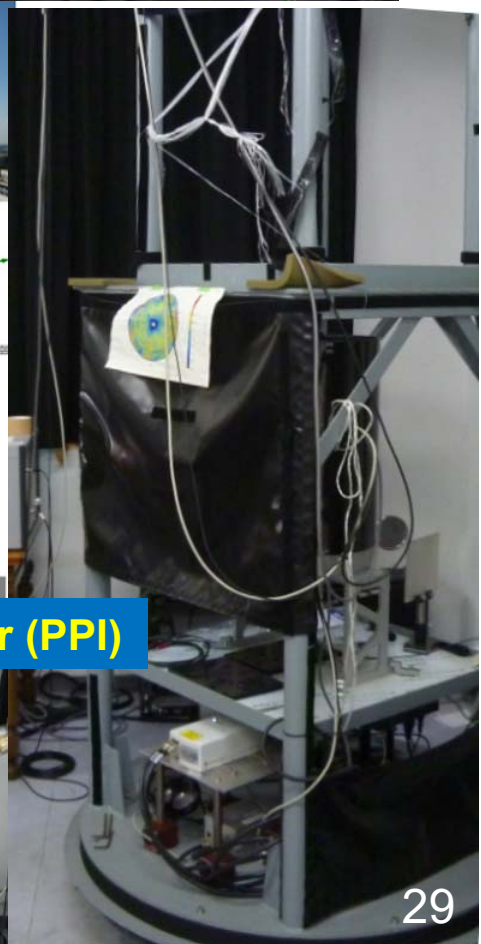

Slant Path 532 nm

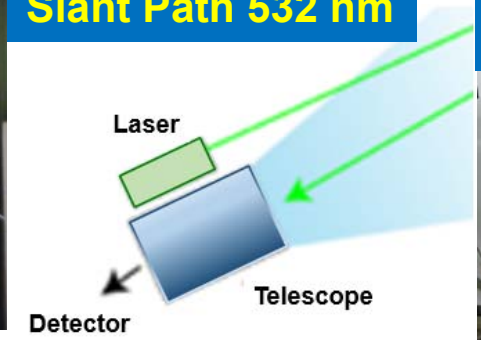

Plan Position Indicator (PPI)

Plan Position Indicator (PPI)

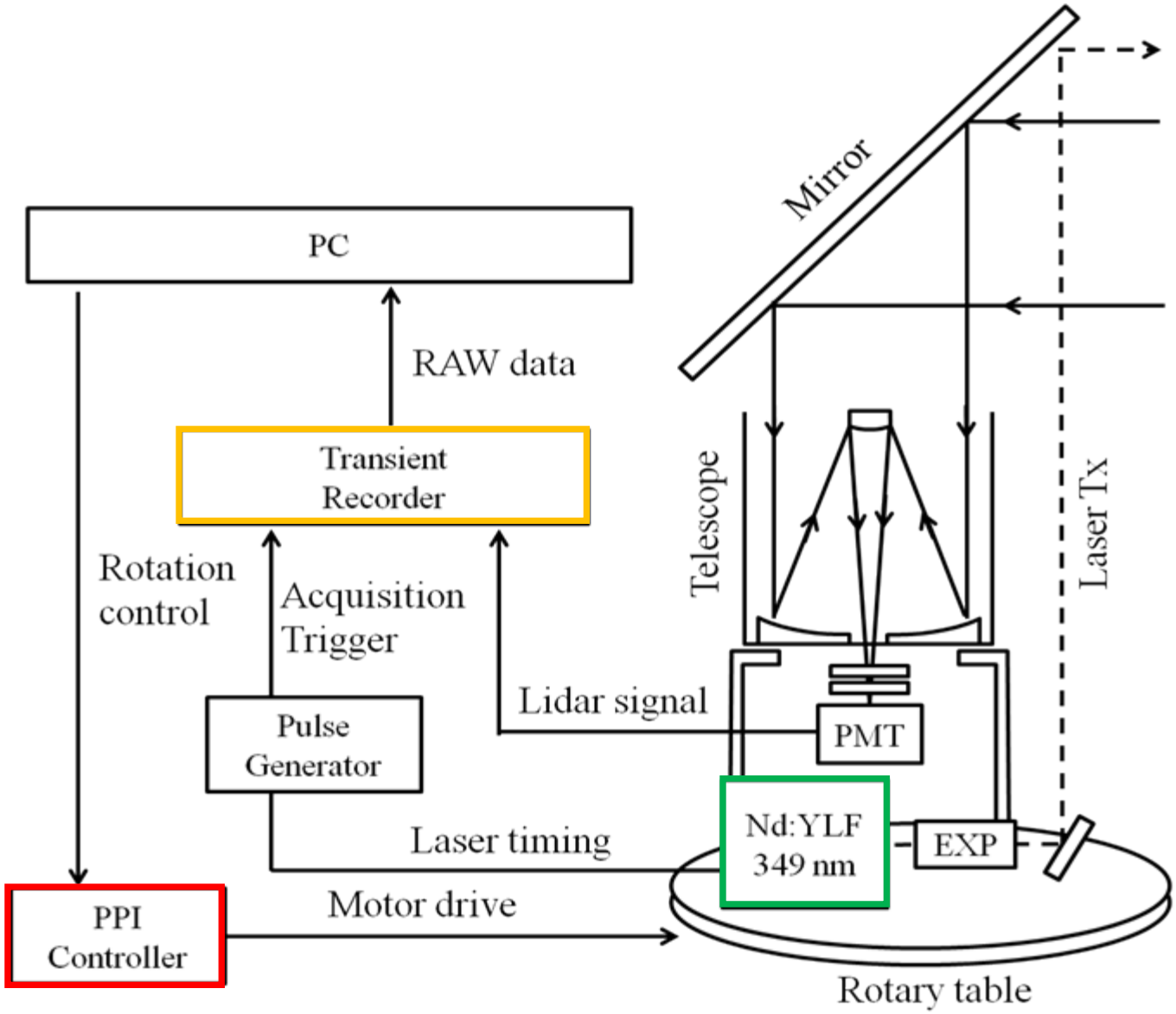

Spatial and temporal variation of aerosol distributions
エアロゾル分布の時間的・空間的な変化

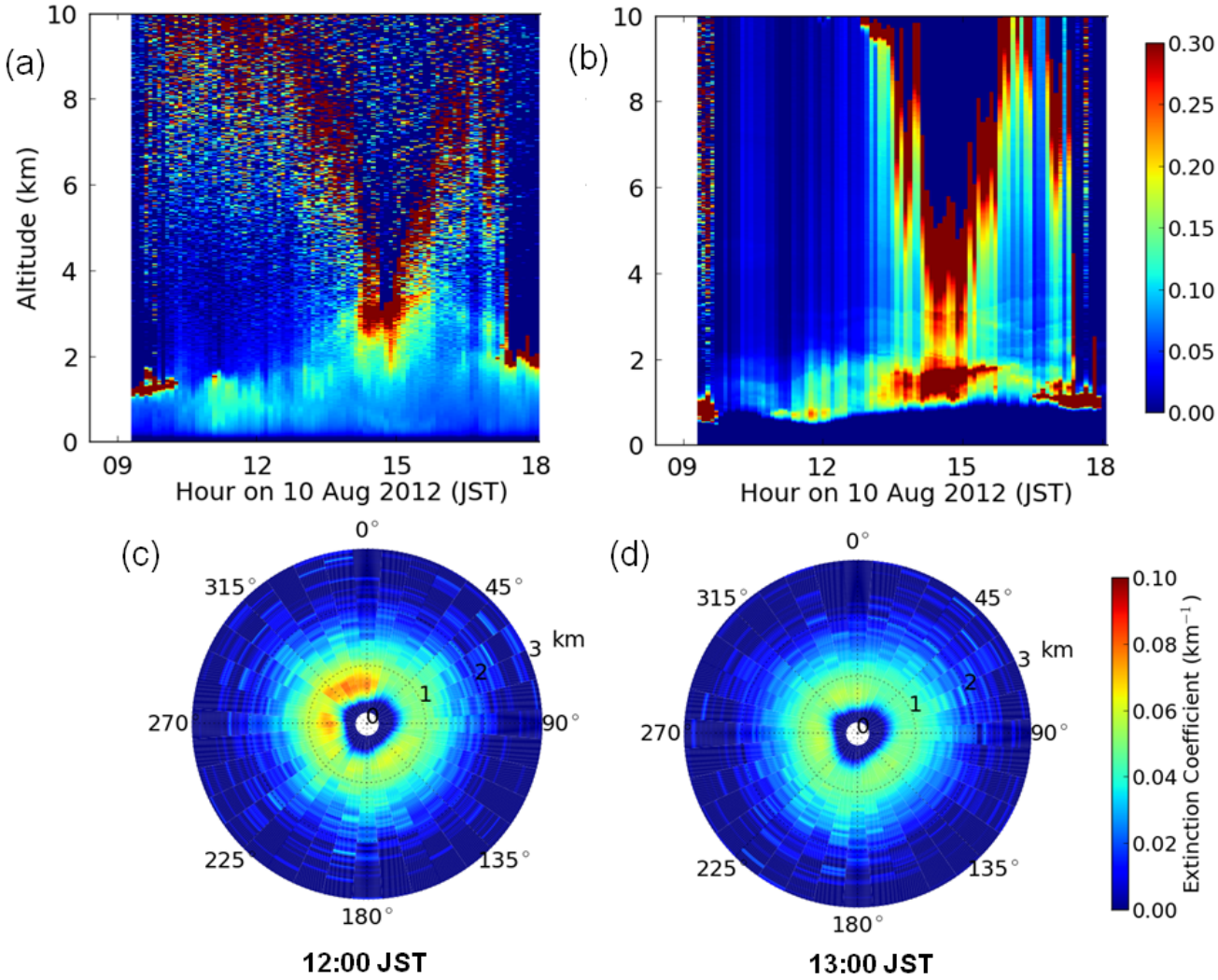

(a) slant-path profile observed at 532 nm.
(b) vertical aerosol profile observed at 532 nm.

(c) horizontal aerosol distribution observed with the PPI unit at 12:00 JST on 10 August 2012, and (d) PPI data observed at 13:00 JST. Each PPI diagram was obtained in a time duration of 30 min.

Instruments for radiation measurement and aerosol sampling

Visibility

Present Weather Detector

Aethalometer

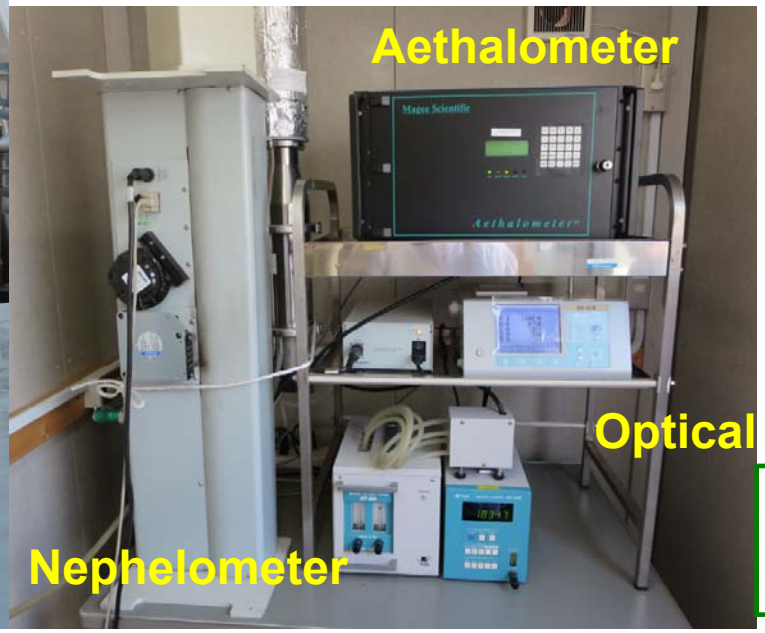

Optical Particle Counter

Nephelometer

Aerosol Optical Thickness

Sunphotometer

Scattering & absorption coefficients, Size distribution

視程 Visibility from PWD

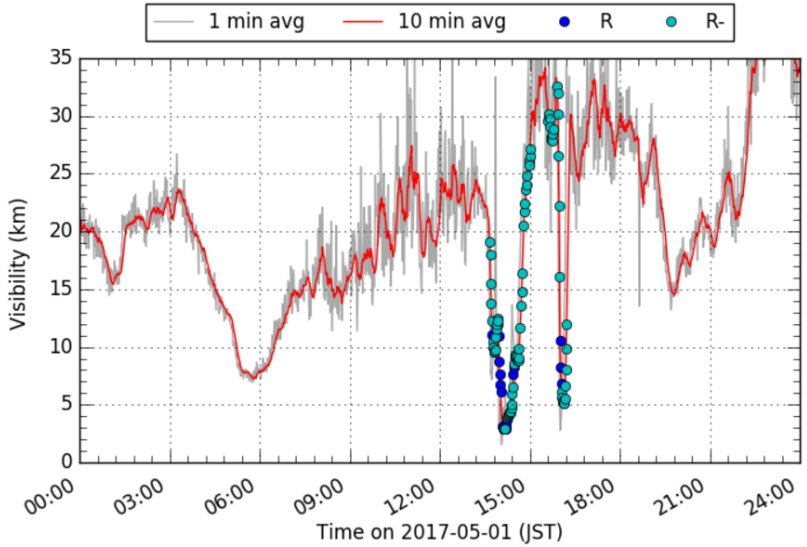

気象情報 Weather Monitor

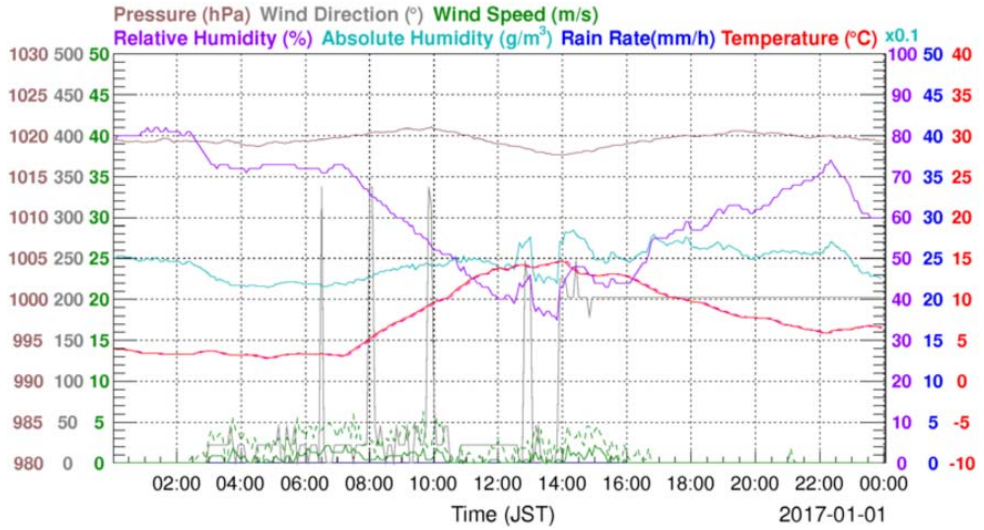

エアロゾル散乱係数

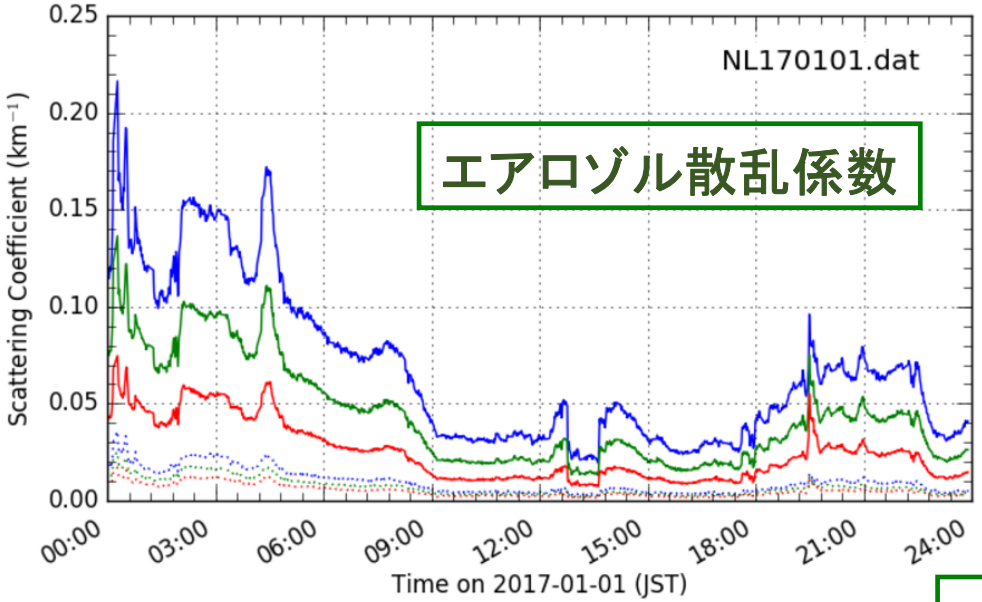

Integrating Nephelometer

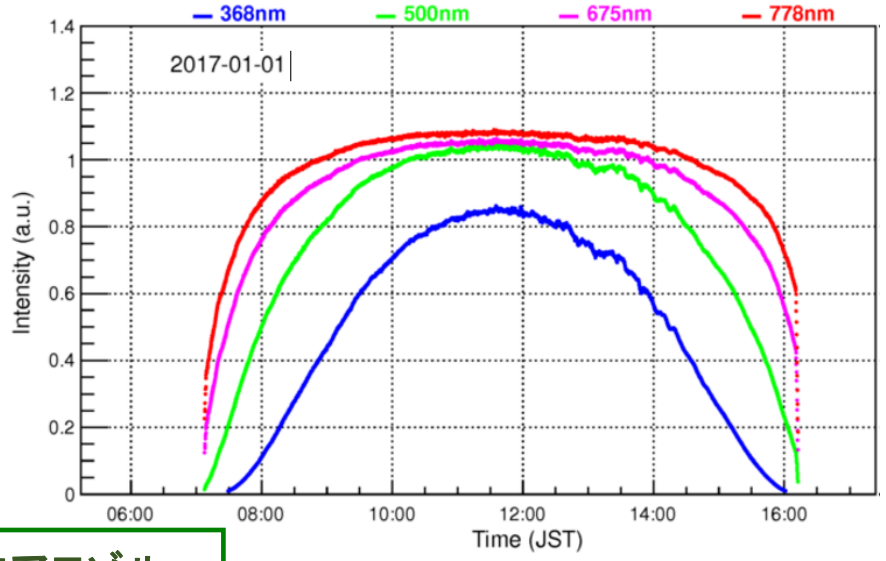

エアロゾル
光学的厚さ
AOT

Sunphotometer

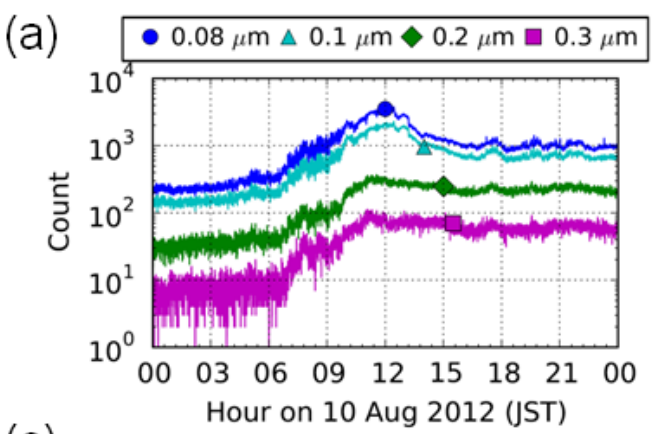

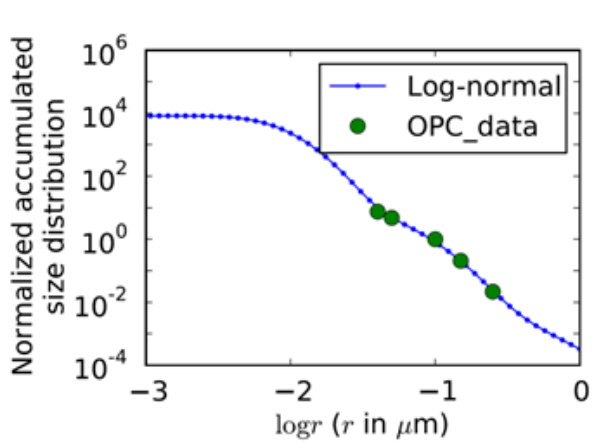

Size distribution data from particle counter

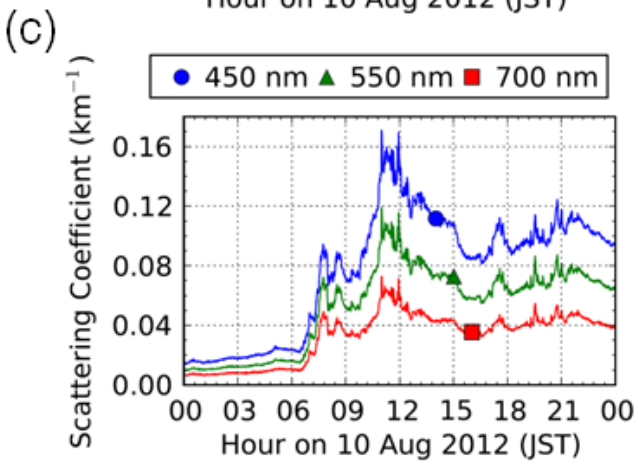

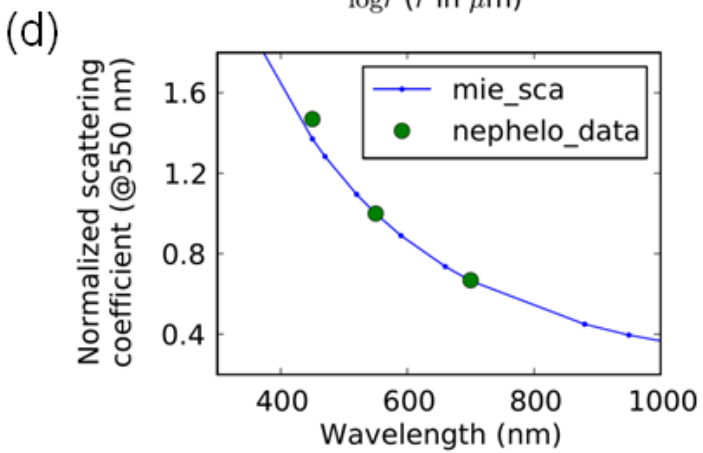

Wavelength dependence of aerosol extinc-tion coefficient

Mie-calculation using the sampling data provides the value of lidar ratio (S_1) as well as the boundary conditions of aerosol extinction.

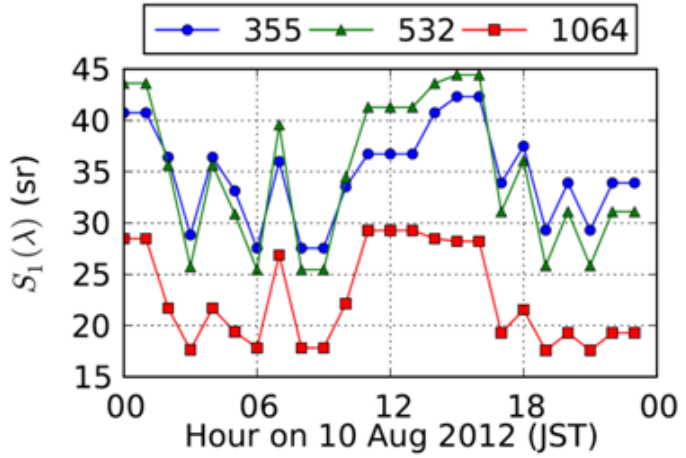

Summary

Environmental remote sensing and lidar activities at CEReS

➢ **Environmental remote sensing studies of CEReS aim at the development of new sensors, synergetic use of satellite and surface observation data, and effective application of RS data to social issues.**

➢ **Two component lidar equation can be solved once the lidar ratio and far-end boundary conditions are provided.**
➢ **For analyzing multi-wavelength lidar, an approach is needed for keeping the consistency of aerosol extinction profiles.**
➢ **Continuous observation of atmosphere was achieved using a portable automated lidar system.**
➢ **Bistatic lidar approach is useful for observing two-dimensional distribution of aerosol particles near the surface level.**
➢ **Coupling the data from ground sampling instruments can provide the constraint at the near-end boundary.**